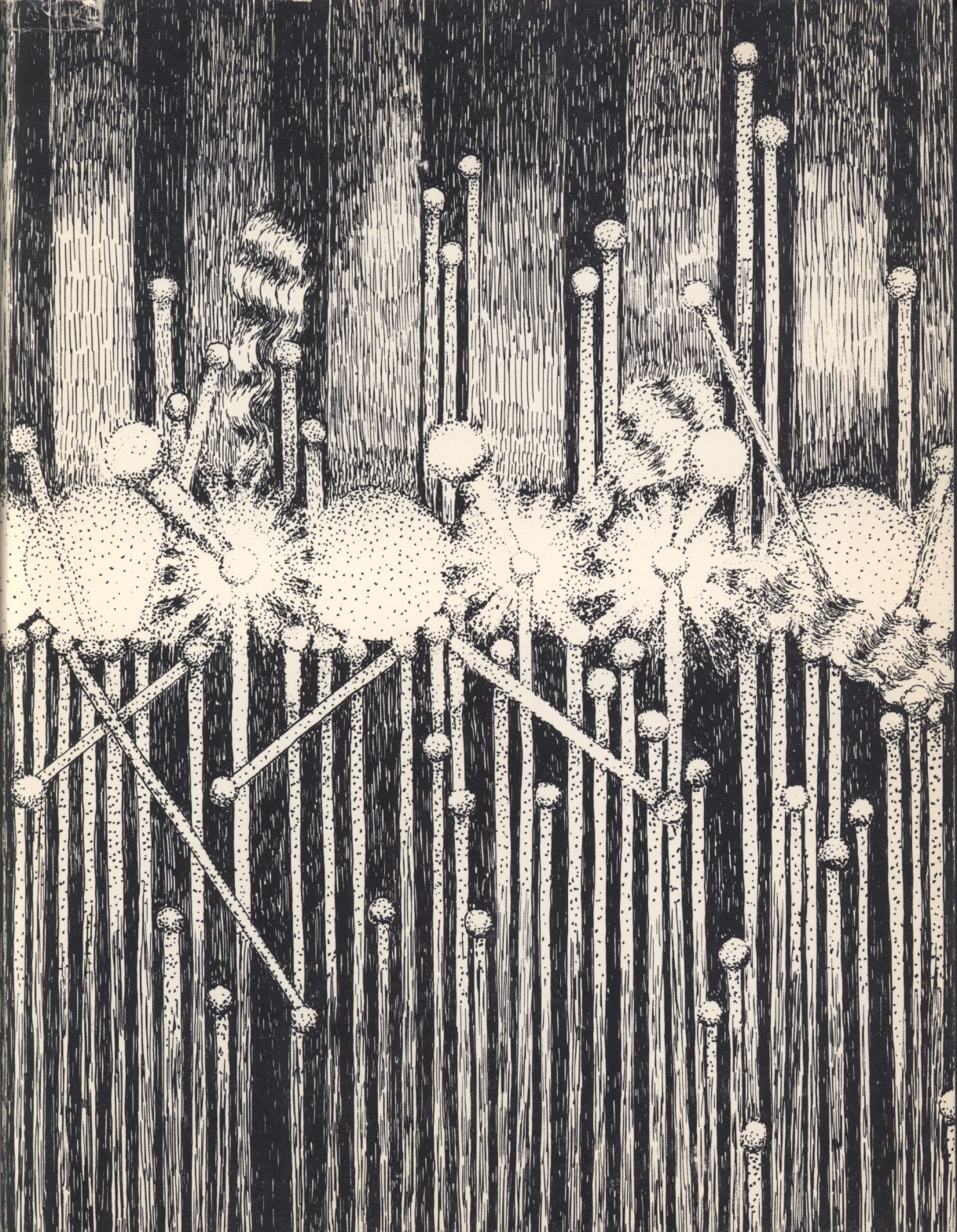

Report of the Group Study on the Electron-Proton Colliding Beam Facility for Fermilab

Fermi National Accelerator Laboratory
Batavia, Illinois

Operated by Universities Research Association
for the United States Department of Energy

PREFACE

In the fall of 1977, I was asked by F. R. Huson, Head of the Accelerator Division, to lead a study to investigate the feasibility of the electron-proton colliding-beams scheme that was proposed at the 1977 Aspen Summer Study. The study took a period of three months (December 1977 - February 1978). The present report is a summary of this study and was prepared during March and April 1978. Obviously the material included is the contribution of many people who are mentioned later, but most of the writeup has been prepared by myself, except Sections III and IV, which have been written respectively by P. Limon and Luke Mo.

Alessandro G. Ruggiero

Fermilab, April 28, 1978

STUDY GROUP PARTICIPANTS

E. Bleser
E. Gray
J. Griffin
D. Johnson
P. Limon
F. Mills
L. Mo
A. Ruggiero
L. Teng

Valuable discussions have been held on various topics with J. Bridges, F. Cole, D. Edwards, G. Nicholls, S. Ohnuma, H. Pfeffer and S. Snowdon.

CONTENTS

		Page
I.	Introduction	1
	A. Opening Remarks	1
	B. History and Backgrounds	2
II.	Outline of the e-p Scheme	5
	A. Introduction	5
	B. Basic Requirements	8
	C. Performance	9
III.	The Physics Potential of e-p	15
	A. Introduction	15
	B. Kinematics	15
	C. Study of the Proton Structure	19
	1. Deep-Inelastic Scattering	19
	2. Electroproduction	24
	3. Photoproduction	28
	D. Weak Interactions	29
	1. Theories of the Weak Interaction	29
	2. Weak Neutral Currents	29
	3. Weak Charged Currents	31
	E. The Detector	34
IV.	The Experimental Set-Up	40
	A. Generalities on the Detector	40
	B. The Non-Magnetic Detector	41
	C. The Magnetic Detector	41
V.	The Electron-Beam Source	48
	A. The Electron Linac	48
	B. Space-Charge Limit	49
	C. The Cooling Ring	50
	1. The Magnet System	50
	2. RF Acceleration	55

Page

3. Radiation Loss and Beam Size at 750 MeV 57

4. Touschek Lifetime 60

VI. Acceleration of Electrons in the Booster 62

VII. Acceleration and Stacking of Protons in the Energy Doubler 68

A. The Proton Beam Characteristics 68

B. Longitudinal Stability and Bunch Area 69

C. Other Instabilities 70

VIII. Acceleration and Storage of Electrons in the Main Ring 72

A. The Collision Region and the Main-Ring Lattice 72

B. Filling of the Two Rings 76

C. Synchrotron Radiation and Electron-Beam Parameters 77

D. Operation of the Main Ring at 4 GeV/c. 79

E. Main Ring Vacuum 83

F. Electron-Beam Lifetime 87

G. Beam-Stability Considerations 90

IX. e-p Colliding-Beam Performance 93

A. The Interaction Region 93

B. Beam Separation 94

C. Luminosity and Beam-Beam Tune Shift 95

D. Operation at Other Energies 98

X. Future Development, Schedule and Cost 101

A. Future Development 101

B. Schedule 102

C. Cost Estimate 103

I. INTRODUCTION

A. Opening Remarks

This report describes a design study for an electron-proton colliding-beam facility at the Fermi National Accelerator Laboratory. This work has been carried out over several years, largely in summer studies[1,2,3,4] in 1976 and 1977 and brought to the conceptual-design stage described in this report by a more concentrated effort over the last six months.

The projected facility will make use of Fermilab accelerators that are already built or presently being constructed. An intense electron beam will be accelerated in the Electron Cooling Ring now being built, then in the Booster, and finally in the Main Ring to an energy of 12 GeV, where they are stored. It will then be brought into collision with an intense proton beam previously accelerated to 1000 GeV and stored in the Energy Doubler/Saver which is planned to be installed in the Main-Ring tunnel. The only new technical components needed for the electron-proton (ep) facility will be a small electron linear accelerator for injection, some beam-transport lines, and a large detector for experiments.

This relatively small investment in the ep facility will enable us to explore a new regime of physics. The great advantages of electrons are that they make the interpretation of experimental results more direct in many cases because they are simpler particles than protons or antiprotons, which are, we have found in the last few years, compound particles with internal structure. This internal structure of the proton can be probed most simply, not by another proton with its internal structure, but by an electron, which does not have such complex structure. It is for these reasons that we have investigated in detail the electron-proton colliding-beam facility described in the following pages.

B. History and Background

The potentials and capabilities of the e-p colliding beam experiments can be understood by drawing a parallel with the earliest experiments on atomic structure. At the beginning of the century it was known that atoms could be broken apart into electrically charged constituents, so that they possessed an internal structure. The scattering experiments of Rutherford were the first means of investigating the internal constituents of atoms. In his experiments, the scattering of alpha particles, produced in radioactive decay, from a thin gold foil was measured. From the scattering, Rutherford was able to deduce that the atom had a dense central nucleus surrounded by electrons.

In modern terms, the success of Rutherford's experiment depended on the fact that the wavelength of the primary radiation, the alpha particles, was small compared with the size of the atom, so that its internal structure could be resolved. In addition, it was important that at the energies available to Rutherford, the alpha particle was a probe without internal structure. It would have been much more difficult to interpret the scattering of gold atoms by gold atoms, for example, because their internal constituents would have given more complicated effects.

In modern experiments we are probing, not the structure of the atom, but of the "elementary" nuclear particles that make it up. The electron offers a probe without internal structure at the energies of interest and thus has advantages analogous to those of Rutherford's alpha particles.

It has been difficult to go as far as we would like with the other crucial parameter, small wavelength. The largest electron energy, that of SLAC (24 GeV), corresponds to a wavelength of 10^{-6} Å, ten times smaller than the nominal size of the proton. Smaller wavelengths are needed to probe the internal structure in more detail.

One way of achieving smaller wavelengths is by raising the energy available in the center-of-mass system by using colliding beams. In the

past a number of electron-positron storage rings and one proton-proton storage ring have been built and used with great success in physics experiments. As yet, there has been no realization of electron-proton colliding beams. There are a number of proposals extant; they are listed in the accompanying table.

Table I-1 Current ep Colliding-Beam Proposals

Proposal	Electron Energy (GeV)	Proton Energy (GeV)	Luminosity (cm^{-2} sec^{-1})
PEP[6]	15	150	10^{32}
ISABELLE[7]	15	200	3.5×10^{31}
CERN[8]	25	270	5×10^{31}
DESY[9]	17.5	280	$\geq 10^{32}$
UNK[10]	20	3000	10^{32}
TRISTAN[11]	16	70/200	6×10^{31}
FERMILAB	12	1000	10^{32}

The consideration of ep colliding-beams systems at Fermilab began with the "Electron Target" proposal[12] of T. L. Collins in 1973, with 3-GeV electrons colliding with 400-GeV protons in the Main Ring. The POPAE (Protons on Protons And Electrons) project[13,14] which was developed soon after, had as one of its features a 20-GeV electron beam colliding with a 1000-GeV proton beam, with a luminosity of $10^{32}/cm^2$-sec.

The possibility of accelerating electrons in the Main Ring was investigated by A. G. Ruggiero[15] in 1973 and in more detail[16] in 1976. There were also investigations by Collins, Ruggiero, and D. A. Edwards[13,17] of accelerating electrons in the Booster. J. K. Walker[18] studied the concept of a third ring, the Accumulator, to be installed in the Main-Ring tunnel. As a result by 1976, the concept of colliding electrons accelerated in the Main Ring with protons accelerated and stored in the Doubler had become quite firmly established. In 1977, J. E. Griffin[4] proposed use of the Electron Cooling Ring as an electron injector to solve the problem of low-energy injection of electrons in the Booster. It is this system that has been developed

and is described in this report.

References (I)

1. D. Berley, et al., Proceedings of the 1976 Aspen Summer Study on the Utilization of the Energy Doubler/Saver, Vol. 1, p. 391.
2. Z. G. T. Guiragossian, Proceedings of the 1976 Aspen Summer Study on the Utilization of the Energy Doubler/Saver, Vol. 1, p. 415.
3. A. Abashian, Proceedings of the 1977 Aspen Summer Study on Colliding Beam Physics at Fermilab, Vol. 2, p. 319.
4. J. E. Griffin, A. G. Ruggiero, Proceedings of the 1977 Aspen Summer Study on Colliding Beam Physics at Fermilab, Vol. 2, p. 337.
5. Fermilab TeV Program, Superconducting Magnet Ring, Fermilab, 1977.
6. PEP Conceptual Design Report, LBL-4288 or SLAC-189 (1976).
7. R. Chasman, Proceedings of the 1975 ISABELLE Summer Study, Vol. II, p. 751, Brookhaven, 1975.
8. R. Billinge, et al., CERN ISR-ES-GE-GS/76-50 (1976).
9. G. A. Voss, et al., DESY PET-77/10, Hamburg, Oct., 1977.
10. V. N. Vapsekov, et al., Proceedings of the X International Conference on High Energy Accelerators, Protvino (USSR) 1977, Vol. I, p. 127.
11. T. Kamei, T. Nishikawa, Proceedings of the X International Conference on High Energy Accelerators, Protvino (USSR) 1977, Vol. I, p. 77.
12. T. L. Collins, Proceedings of the 1973 Aspen Summer Study on Colliding Beams, Vol. 2, p. 97.
13. T. L. Collins, et al., TM-600, Fermilab, Aug., 1975.
14. A 1000-GeV on 1000-GeV Proton-Proton Colliding Beam Facility, Fermilab, May, 1976, Appendix I, p. 139.
15. A. G. Ruggiero, TM-431, Fermilab, 1973.
16. A. G. Ruggiero, D. E. Johnson, TM-693, Fermilab, 1976.
17. D. A. Edwards, Unpublished note, Fermilab, 1975.
18. J. K. Walker, TM-432, Fermilab, 1973.

II. OUTLINE OF THE e-p SCHEME

A. Introduction

The first electron-proton schemes considered at Fermilab were constrained to allow simultaneous operation with fixed-target experiments. This simultaneous operation is possible either with the addition of a third ring for the electron beam or by injecting protons directly into the Energy Doubler at 8 GeV, which assumes that the quality of Energy Doubler magnets remains good at very low fields from the Booster. This scheme would free the Main Ring for the use as an electron storage ring.

More recently, during the study of pp and $\bar{p}p$ colliding-beam systems at Fermilab[1,2], which can involve crossings between the Energy-Doubler and the Main Ring, it appears that it might be desirable to have both rings devoted to colliding-beam experiments. Internal-target experiments would still be possible in this mode of operation. The e-p scheme proposed here is based on the assumption of a reasonable fraction of time devoted to colliding beams. Thus the difficulties of a third ring or 8-GeV injection in the Doubler are avoided.

The scheme, sketched in Fig. II-1, works as follows. Protons are accelerated as usual in the Booster to 8 GeV, transferred to the Main Ring in 13 batches and accelerated to 100 GeV. At this energy, they are extracted and injected into the Energy Doubler. If desired, more 100-GeV pulses can be stacked in momentum phase space. Finally, the beam is accelerated to 1000 GeV, where the Energy Doubler is converted to the storage mode (beam storage is possible for several hours) and the proton beam is kept bunched at the standard frequency of 53.1 MHz. All the steps involved in this process have already been studied in connection with the pp and $\bar{p}p$ colliding-beam schemes[1,2,3] and appear to be feasible. A list of beam parameters is given in Table II-1. The time to accelerate and store this beam is approximately one minute. After this operation is completed, the Main Ring is available for the electron beam.

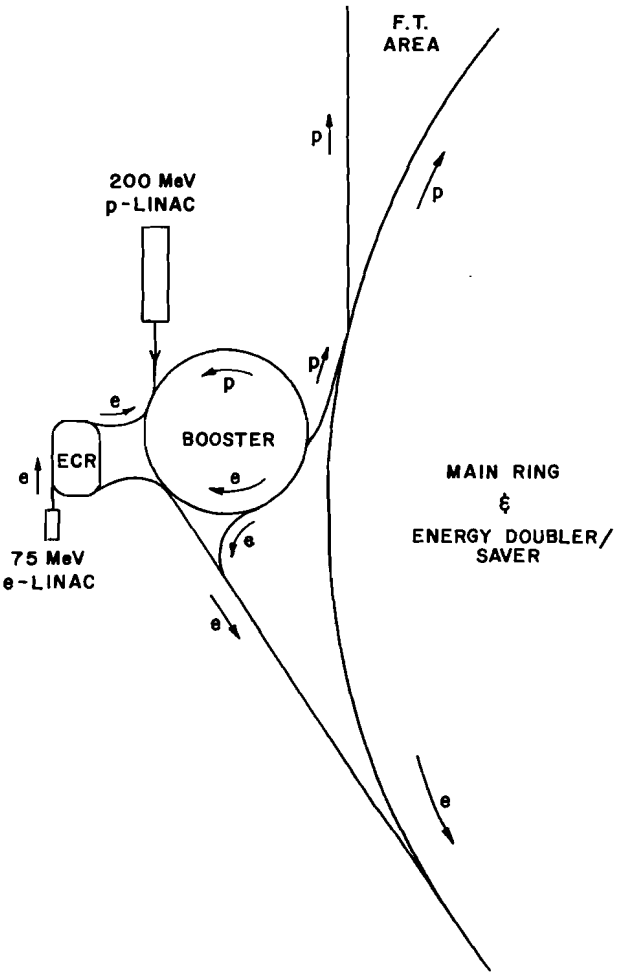

Fig. II-1. The e-p Scheme Layout

Table II-1. 1000-GeV Proton-Beam Parameters

(Energy Doubler)

Intensity	0.15 to 1.5 A
No. of Pulses from Main Ring	One to 10
No. of Bunches	1113
Accelerating Frequency	53.1 MHz
RF Voltage	1 MV
Emittance ($\epsilon_x = \epsilon_y$, 95% of beam)	$0.013\ \pi\ 10^{-6}$ m
Longitudinal phase space area	3.8 eV•s (with 10 pulses)
Bunch length (σ, rms)	50 cm (with 10 pulses)
Bunch height ($\delta p/p$, rms)	1.2×10^{-4}
No. of protons/bunch	2×10^{11} (with 10 pulses)
Total No. of protons	2×10^{14} (with 10 pulses)

For the second part of our scheme, we assume that a 75-MeV electron linac is attached to the Electron Cooling Ring presently under construction.[4] This ring is ultimately to be used for the production of an intense antiproton beam and its location at the Booster is mainly governed by this requirement. The electrons are accelerated in the Cooling Ring to 750 MeV and transferred to the Booster, in which they are accelerated to 4 GeV and transferred to the Main Ring, where they are stored. This cycle is repeated several times until the Main Ring has been completely filled in box-car fashion. After the Main Ring is filled, the entire electron beam is accelerated to an energy between 11 and 12 GeV, an energy limit set by the available rf power in the Main Ring. During all these steps of the process of producing the 12-GeV electron beam, a constant accelerating frequency of 53.1 MHz can be used. This corresponds to 24 bunches accelerated each pulse in the Cooling Ring and in the Booster; 48 such pulses are required to fill the Main Ring. The electron-beam parameters are given in Table II-2.

Table II-2. Electron-Beam Parameters

(Main Ring)

Energy	11-12 GeV
Intensity	0.38 A
No. of Pulses from Booster	46
No. of Bunches	1113
Accelerating Frequency	53.1 MHz
RF Voltage	4 MV
Emittance (95% of beam, full coupling)	$0.3\pi\ 10^{-6}$m
Energy Spread ($\delta E/E$, rms)	6×10^{-4}
Bunch Length (σ, rms)	13 cm
No. of electrons/bunch	5×10^{10}
Total No. of electrons	5×10^{13}

B. Basic Requirements

The trajectories of the electron and proton beams are shown by arrows in Fig. II-1. In addition to an electron linac with its housing, power supply and shielding, a transport line from the linac to the Cooling Ring must be supplied, as well as an injection kicker. The electrons will circulate in the clockwise direction in the Cooling Ring (like the antiproton beam). They can be extracted from the Cooling Ring and injected into the Booster by use of the same extraction kicker and transport line used for the antiproton beam. A new rf cavity and a new magnet power supply are required for acceleration of the electron beam, because the present design of the electron cooling ring does not contemplate acceleration. The direction of circulation in the Booster, that is, whether the field has to be reversed or not, will be determined by the $\bar{p}$-beam production requirements. The same is true of extraction from the Booster, transport and injection to the Main Ring. The additions or modifications that are required to produce a 12-GeV electron beam circulating in the Main Ring are:

(i) A 75-MeV electron linac.

(ii) Linac housing and shielding.

(iii) Linac power supply.

(iv) Transport line from Linac to the Cooling Ring.

(v) A 40-kV, 53-MHz, 20-kw rf system (cavity, power supply and amplifier).

(vi) A new power supply for ramping the Cooling Ring magnets.

(vii) An injection kicker in the Cooling Ring (200 G, approximately about 1m long, and 10 nsec risetime).

(viii) Radiation shielding of the Cooling Ring. (The beam energy is only 140 J.)

(ix) An injection kicker in the Main Ring with a very short risetime, capable of operating for 50 pulses at a repetition rate that will depend on the repetition rate of the Cooling Ring.

(x) Cooling of the Main-Ring rf system to operate cw at 4 MV.

(xi) The capability of ramping the Main-Ring magnet system from 4 GeV to 12 GeV. This also includes the correction-elements packages.

In the third and last part of our scheme, the electron and proton beams are made to collide in a properly designed interaction region that uses one of the six long straight sections.

C. Performance

The Energy Doubler superconducting magnets will be installed just underneath the Main Ring as shown in Fig. II-2, with a vertical separation of 25 in. To make the two beams collide with each other, the two rings are to be moved vertically together in a long straight section. A local vertical bypass will be added to the Main Ring to bring the electron beam down to the level of the proton beam in the Doubler, as shown in Fig. VIII-1. To avoid collisions of bunches next to those colliding in the middle of the interaction region, the two beams will collide at a small horizontal angle. Finally, a low-β insertion will be added to both the Main Ring and the Doubler to increase the luminosity. Smaller electron-beam emittances can be obtained by increasing the betatron tunes of the Main Ring to approximately 27, which is within the quadrupole capabilities at the electron-beam energy of 12 GeV.

Performance parameters are given in Table II-3. Observe that the electron beam energy has been chosen to be 11.5 GeV to allow a

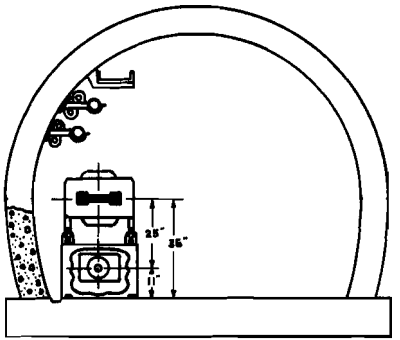

Fig. II-2. Location of the Superconducting Ring in the Main Ring Tunnel.

reasonably long quantum lifetime without increasing the available Main-Ring rf voltage, 4 MV.

Table II-3. e-p Colliding-Beam Performance

	e	p
Energy	11.5 GeV	1000 GeV
β_x^*	0.35 m	5 m
β_y^*	0.30 m	5 m
η_x^*	0.01 m	0.7 m
η_y^*	-0.06 m	----
$\nu_x \sim \nu_y$	26.7	20.4
Crossing angle	2 mrad	
Luminosity	$\sim 10^{32}$ cm^{-2}s^{-1}	
$\Delta\nu$, Beam-Beam Tune Shift	0.02	0.001

The luminosity as a function of the electron-beam energy is shown in Fig. II-3, and as a function of the proton-beam energy in Fig. II-4. The larger electron energies shown would require more rf voltage in the Main Ring. The slope of the luminosity for these energies is calculated under the assumption that more rf voltage is available, but that the power delivered to the beam is kept constant, which means that the beam intensity is lowered. The luminosity also increases when the electron-beam energy is decreased if the beam intensity is kept constant. This increase is caused by a reduction of the beam emittance, which also allows a smaller crossing angle. Note that we are far away from the beam-beam tune-shift limit for the proton beam. The luminosity is decreased slightly by reducing the proton beam energy, mainly because of the increase of the proton beam size.

Because of the available rf voltage, only one colliding-beam insertion is possible, and there can therefore be only one experiment at a time. In fact, each insertion gives a need for extra rf power because

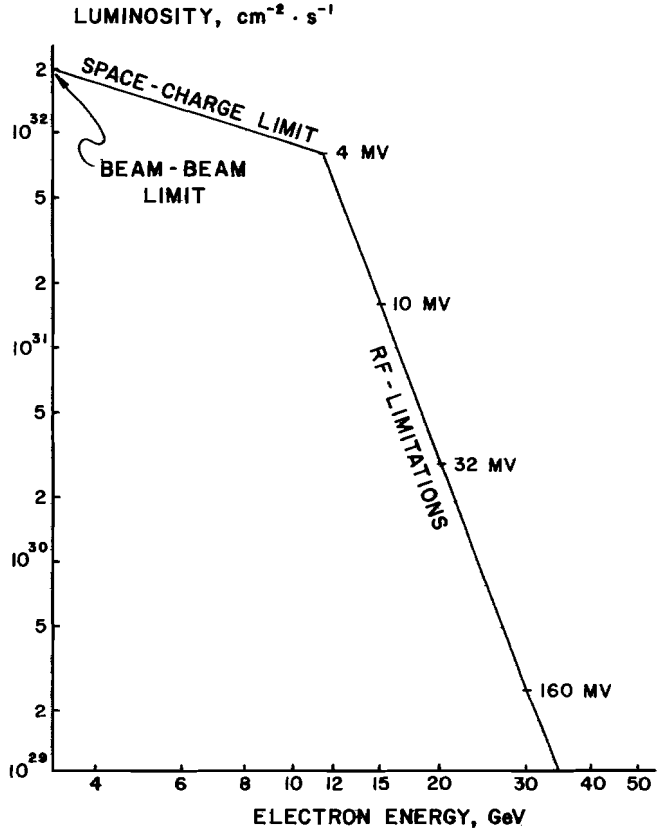

Fig. II-3. Luminosity versus Electron Beam Energy

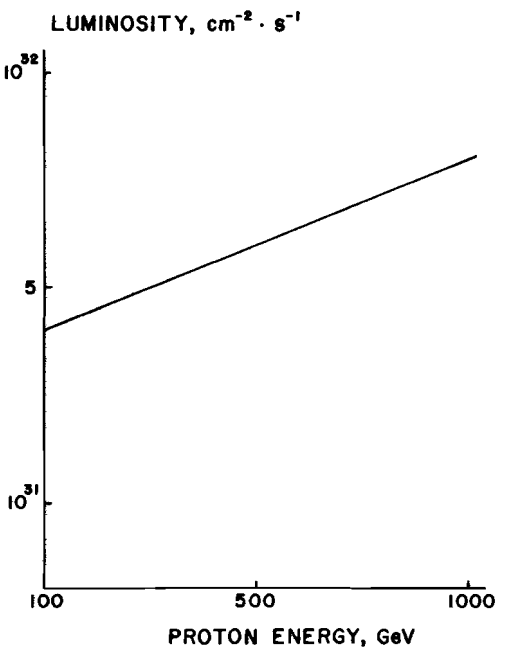

Fig. II-4. Luminosity versus Proton Beam Energy

of the strong vertical bending to move the Main-Ring beam to the elevation of the Energy Doubler.

References (II)

1. Proceedings of the 1977 Aspen Summer Study on Colliding Beam Physics at Fermilab.
2. Fermilab TeV Program, Superconducting Magnet Ring, Fermilab, 1977.
3. A. G. Ruggiero, TM-727, Fermilab, 1977.
4. Design Report of the Fermilab Electron Cooling Experiment, Fermilab, Nov., 1977.

III. THE PHYSICS POTENTIAL OF e-p

A. Introduction

The existence of electron-proton colliding beams would open up kinematic regions in the study of lepton scattering that cannot be reached by any other presently imaginable technology. In the following sections, we will use the parameters of the e-p rings described above to estimate the rates of various processes we believe we can study. This discussion is not exhaustive, but is meant merely to give an idea of what can or cannot be done. Details of the theory are available in many excellent reviews[1-5], and the reader is encouraged to study them. In Section B of this chapter, we will attempt to familiarize the reader with the notation used and the unusual kinematics that dominate the design of a detector for e-p colliding beams. The next two sections, C and D, are a brief discussion of proton structure and weak interactions, respectively.

B. Kinematics

The kinematic variables commonly used in e-p scattering are defined in Fig. III-1.

The e-p experiment is characterized by the large asymmetry in the scattering momenta. In most of the kinematic region, the electron is back-scattered at very large momentum, and the hadron fragments are along the beam direction. Only the "photon" fragments are at large lab angles, or at least in the forward hemisphere, with respect to the incident electron. Figure III-2 shows this effect most clearly. Here we have plotted p_t' of the outgoing electron along lines of constant Q^2 and W. Even at Q^2 as low as 1000, the electron is back-scattered.

Figure III-3 shows the same plot for the hadron system, which is even more collimated. It is clear from these two polar plots that a detector must be able to cover very small angles along the direction of the incident proton. The photon direction, however, is in the opposite hemisphere, and at small x, at least, is at rather large angles. This

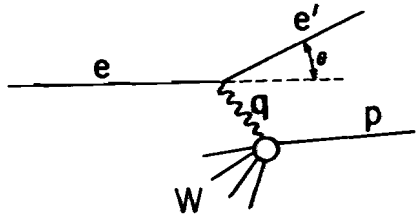

$e = (E, E, 0, 0)$ = incident-electron four momentum

$e' = (E', E'\cos\theta, E'\sin\theta, 0)$ = scattered-lepton four momentum

$p = (E_p, -E_p, 0, 0)$ = incident-proton four momentum,

$$Q^2 = -q^2 = (e-e')^2 = 4\ EE'\sin^2\frac{\theta}{2},$$

$$\nu = \frac{p\cdot q}{m_p} = \frac{2E_p}{m_p}\left(E-E'\cos^2\frac{\theta}{2}\right),$$

$$W^2 = (q+p)^2 = 2\ m_p\nu + m_p^{\ 2} - Q^2,$$

$$S = (e+p)^2 = 4\ EE_p + m_p^{\ 2},$$

$$\nu_{max} = \frac{S-m_p^{\ 2}}{2\ m_p}$$

and

$$x = \frac{Q^2}{2\ m_p\nu} \qquad y = \frac{\nu}{\nu_{max}}.$$

Fig. III-1. One Photon Exchange Kinematics.

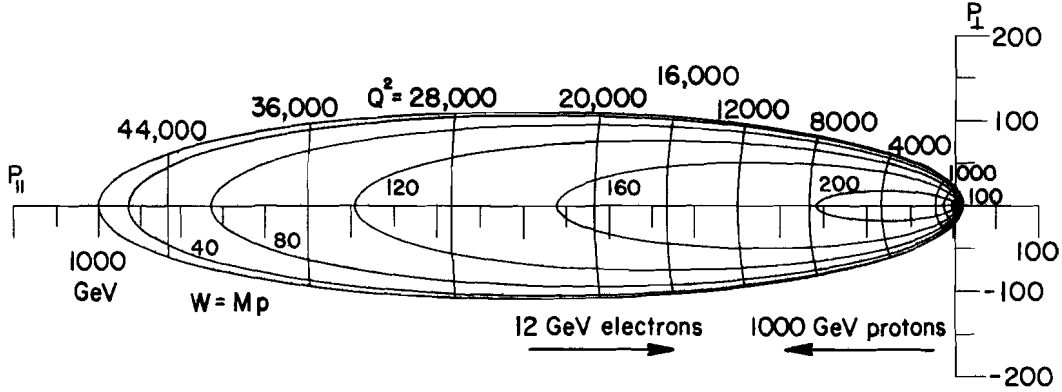

Fig. III-2. Polar Diagram of Outgoing Electron Kinematics.
(Lines of Constant Q^2, W)

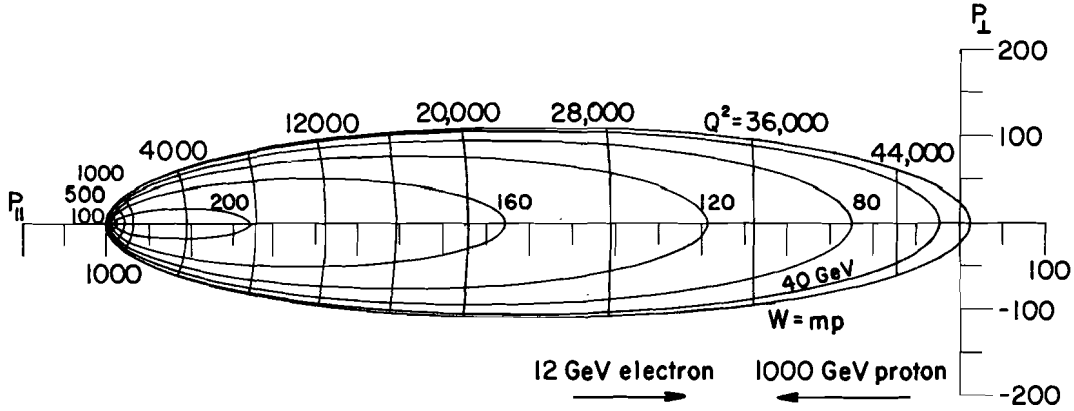

Fig. III-3. Polar Diagram of Outgoing Hadron Kinematics.
(Lines of Constant Q^2, W)

is shown in Fig. III-4. Some of the kinematic variables are more easily seen in another sort of diagram. Figure III-5 shows the kinematic boundaries, along with lines of constant E'_e, θ'_e, and P_t. It is worth noting again that the scattered electron is at large backward angles and very high energy. The form of the detector will be dominated by kinematics, and is quite insensitive to changes in theories and models.

C. Study of Proton Structure

1. Deep-Inelastic Scattering. It has long been thought that the electron is the best particle to probe the internal structure of the nucleon. One can consider that large Q^2 means probing at small distances and that the electron, in addition, is a simple particle, unlike the nucleon. In the context of that view, e-p colliding beams are unsurpassed as microscopes, able to resolve to distances of the order of 10^{-16} cm.

Present-day μ-scattering experiments have reached $Q^2 \lesssim 50\ (\mathrm{GeV/c})^2$. With the advent of the Energy Doubler, Q^2 might go as high as 500 $(\mathrm{GeV/c})^2$. A 12-GeV electron beam colliding with a 1000 GeV proton beam has a kinematic limit of $Q^2 = 48{,}000\ (\mathrm{GeV})^2$, and can collect statistically significant data at Q^2 values of 20,000 $(\mathrm{GeV})^2$. There are many theoretical models of nuclear structure which can describe the existing low Q^2 data. We hope the data in the Q^2 regime which can only be reached with e-p collisions will distinguish among them. Of course, as is always the case when a new energy region is opened up, the probable result will be entirely new and unexpected physics.

Figure III-1 shows the Feynman graph for one-photon exchange. The cross section for this process can be written quite generally in terms of two dimensionless structure functions F_1 and F_2 as

$$\frac{d^2\sigma}{dxdy} = \frac{4\pi\alpha^2}{Sx^2y^2} \left[(1-y)F_2(x,Q^2) + y^2xF_1(x,Q^2)\right] . \qquad \text{(III-1)}$$

In models in which partons of spin ½ are the constituents of the proton,

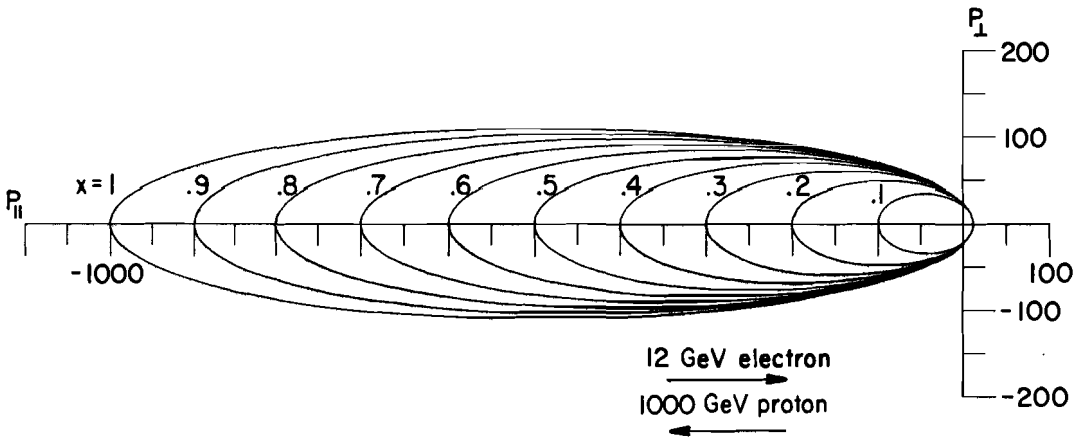

Fig. III-4. Polar Diagram of "Current Fragmentation". (Lines of Constant x)

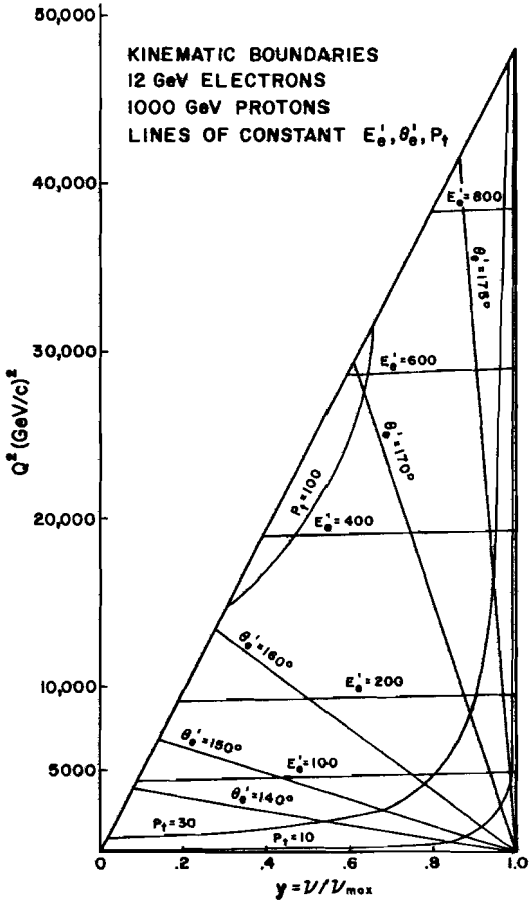

Fig. III-5. Kinematic Boundaries. (Lines of Constant E_e', θ_e', P_t)

the structure functions are related by the Callan-Gross relation

$$F_2 = 2xF_1. \qquad \text{(III-2)}$$

In the low Q^2 region, so far experimentally examined,
ing is found approximately held to 20%. In the limit of perfect scaling

$$F_i(x,Q^2) = F_i(x), \quad (i = 1,2) \qquad \text{(III-3)}$$

independent of Q^2. We use this as a starting point for our rate calculations.

Figure III-6 shows the rate per day (24 hours) at a luminos- of 10^{32} $cm^{-2}sec^{-1}$ in bins of dxdy of 0.04. In fact, there have been some cuts made on these (theoretical) data. We have required that $P_t' \gtrsim 10$ GeV/c, and $\theta_e^{lab} \gtrsim 90°$, (electron scattered backward in the lab). In these calculations we have taken $F_2(x)$ from the analysis of Barger and Phillips.[6] Note that in the limits of perfect scaling there are significant numbers of events at Q_2^2 values of the order of 10^4 $(GeV/c)^2$.

Experimentally, we know already that Bjorken scaling does not hold exactly. Furthermore, the way in which scale breaking occurs provides clues as to the particular theory that could best describe the phenomenon. Scale breaking in gauge theories is like $\left[\ln(\frac{Q^2}{\lambda^2})\right]^{-\gamma}$, where γ is a calculable parameter that depends on the particular model of the nucleon. Other field theories find scale breaking of the form $(\frac{a}{Q^2})^{\beta}$, where β is in general not calculable. Because of the slow variation and because polynomials can look like logarithms over a wide range of variables, it is of primary importance to go out to the highest Q^2. Only in this way can one make definitive tests of the theories. Table III-1 shows some representative functions as a function of Q^2. The logarithmic function is from an asymptotic-freedom model with four colors of quarks, while the other functions are adjusted to mimic with the logarithmic function between Q^2 limits of 2 and 30 $(GeV/c)^2$.

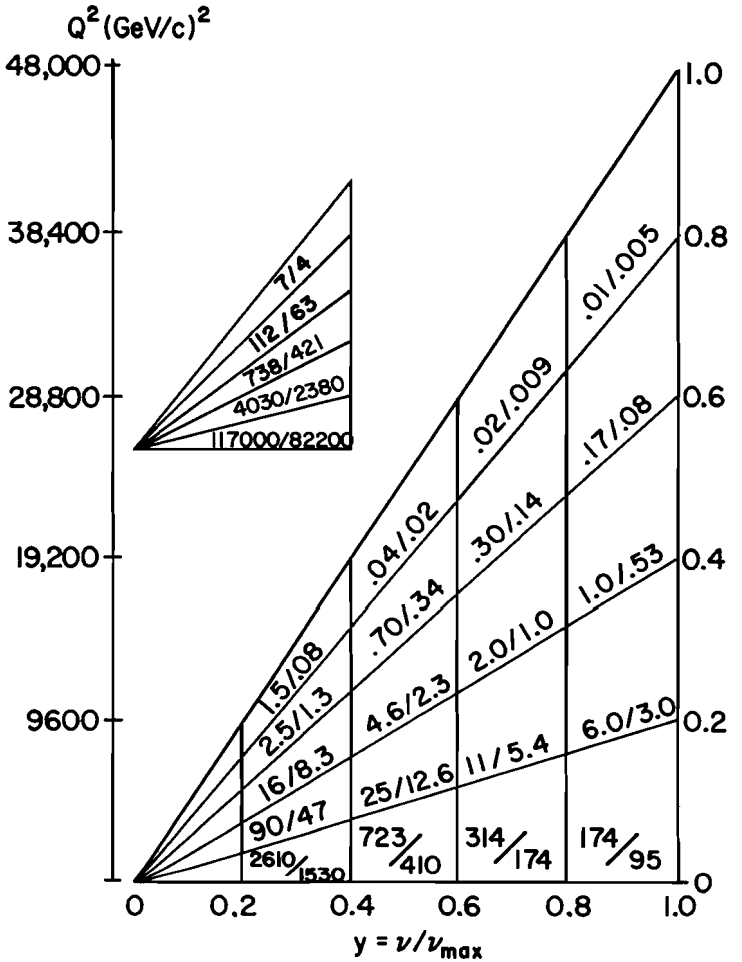

Fig. III-6. Rates for One Photon-Exchange.
Perfect Scaling with Cuts.

Table III-1. Possible Forms of Scaling Violation[2] in νW_2

Q^2, $(GeV)^2$	2	30	100	2000	10000
$\left(\frac{\ln 8}{\ln 4Q^2}\right)^{.43}$	1	.7	.63	.53	.50
$\left(\frac{2}{Q^2}\right)^{.13}$	1	.7	.60	.41	.33
$\left(\frac{143}{141+Q^2}\right)^2$	1	.7	.35	4.5×10^{-3}	2×10^{-4}

Figure III-7 shows the number of events with $Q^2 \geq Q_o^2$ per day under the assumptions of scaling and with $F_2(x,Q^2)$ modified by the asymptotic-freedom function of Table III-1. Another way to look at this[1] effect is shown in Figs. III-8 and III-9. Here the asymptotic-freedom result mentioned previously is plotted as a function of Q^2 in curves of constant x. In this particular model, we can see a number of features:

(i) The cross section is increased at small x by a large amount. It decreases at high x, but the rate is decreasing in this region anyway due to propagator effects.

(ii) The structure function changes most rapidly in the region of modest Q^2 and levels out at high Q^2. This may turn out to be important, since it would allow us to separate easily the effects due to scale breaking from effects due to weak interactions.

2. Electroproduction. In a simple picture of electron-proton scattering, a virtual photon of momentum $\vec{q}$ strikes a parton constituent of a proton with a fraction x of the total momentum of the photon. The momentum of this "current-fragmentation jet" is then $\vec{q}+x\vec{p}$. Over a large region of the kinematic plot, this jet is at large lab angles, well separated spatially from the scattered lepton, and from the proton jet, which is along the proton direction. It is important to note that the energy and angle of the current jet is completely determined by the

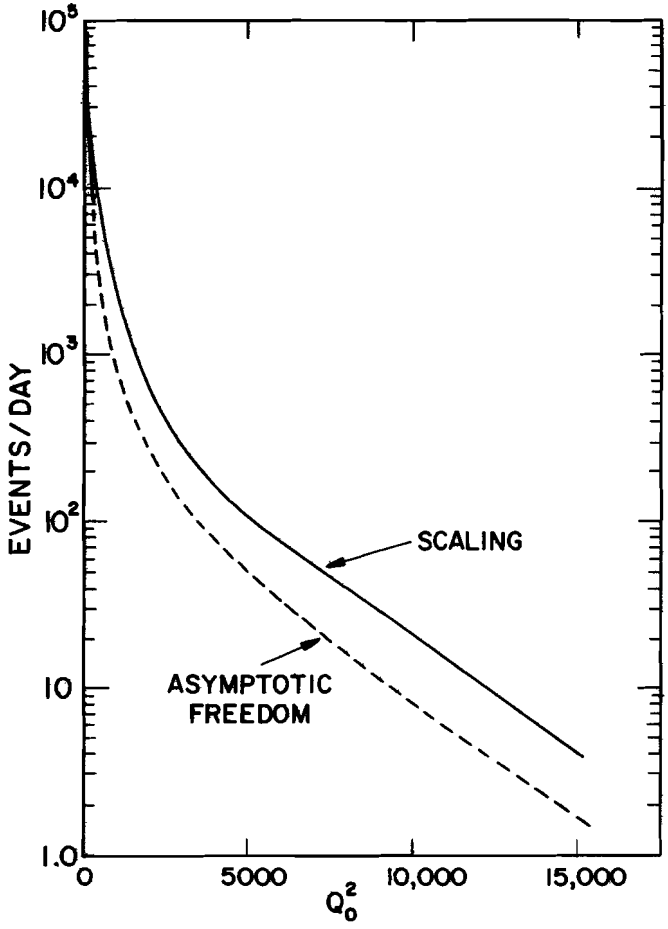

Fig. III-7. Rates for $Q^2 > Q_0^2$/day with Two Types of Scaling Violation and Cuts.

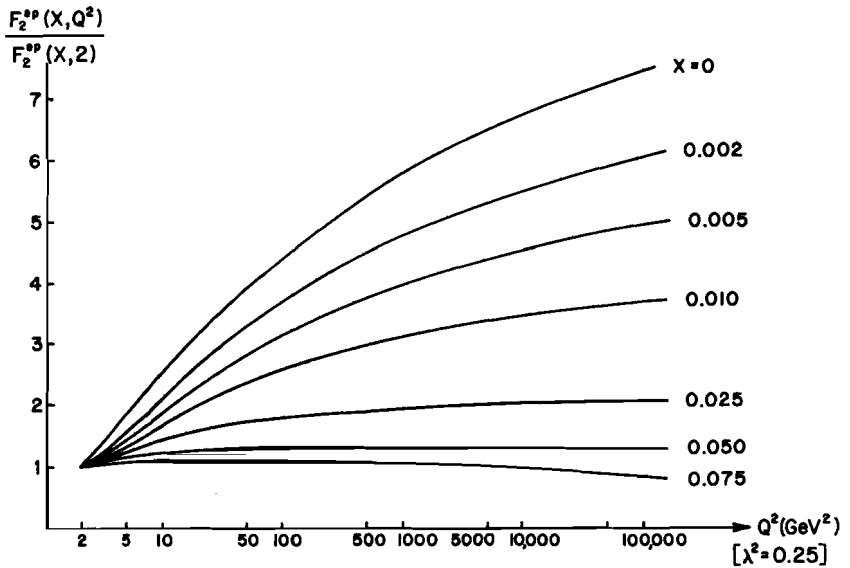

Fig. III-8. Constant x-Curves vs. Q^2 with Asymptotic Freedom Scaling Violations. Small x.

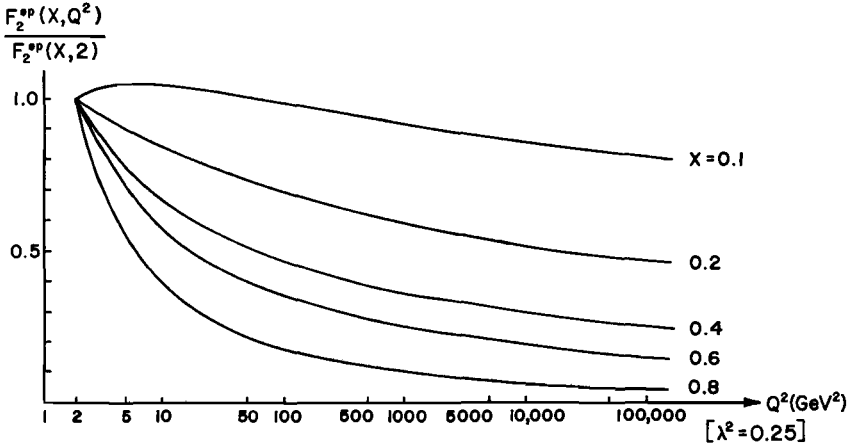

Fig. III-9. Constant x-Curves vs. Q^2 with Asymptotic Freedom Scaling Violations. Large x.

kinematics of the scattered electron. What is not known, of course, is the momentum distribution of the quarks. Some models, such as those of Politzer[7] and Feynman, Field and Fox[8] predict the jet will have large internal transverse momenta at high Q^2 and might even have additional jets due to the bremsstrahlung of gluons. What is clear is that there is a rich lode of physics to be mined. In addition to studying the gross structure of the jet, these experiments might be a source of new quarks. This is particularly true in the low x and high y region where the "sea" of quark-antiquark pairs dominates. The photon may give enough momentum to break up this pair and send the new quark into the current jet. Since the sea of quark-antiquark pairs might have all of the quark flavors included, we could have a relatively large cross section for the production of new flavors. Furthermore, these events will put the new quarks into a relatively clean region in the detector, at momenta that are low compared with the other fragments. This means that a magnetic detector can be used to best advantage in reconstructing the masses and particle types in the current jet.

3. Photoproduction. Electroproduction turns into photoproduction in the limit $Q^2 \to 0$. The "nearly real" photons can be obtained by tagging the outgoing electrons at very small angles and obtaining a photon beam of known energy. This constraint loses a large factor in luminosity, due to $\theta_{e_{min}}$ perhaps of the order of

$$L_{\gamma p} \simeq 10^{-3} L_{ep}$$

A non-tagged beam might be more intense by a factor of 20 or so. One obvious experiment is to look along the photon direction for the diffractive production of vector mesons. In principle, masses as high as 150 GeV can be produced for $|t_{min}| \leq 0.2$ GeV^2. On the other hand, the cross section for production of vector mesons is expected to decrease like $1/M_V^4$. In this case, the event rate will be approximately one event/day at M_V=40 GeV. As in the electroproduction experiments, the

decay products are expected at large angles and can easily be analyzed with magnetic detectors.

D. Weak Interactions

1. Theories of the Weak Interaction. It is of primary importance that the weak interactions be investigated at high Q^2. If the weak interaction continues to grow linearly in S, as it does at small S, it will be comparable to the electromagnetic interaction at $Q^2 \approx 5000\ (\mathrm{GeV/c})^2$. There is a strong prejudice for a description of the weak interaction that does not continue to grow with energy. Recently, the most popular theories advocate the high mass intermediate bosons which supposedly damp the weak interaction when Q^2 is greater than the square of this mass. At very high Q^2, the weak interaction behaves much like the electromagnetic interactions, in these theories, but may be even greater in magnitude. One of these theories, by Weinberg and Salam, has already had many experimental successes, the prediction of weak neutral currents in neutrino interactions being the most dramatic. There are also some contradicting experiments, namely atomic-physics experiments looking for parity violation in neutral currents in bismuth.

It appears from present data, if the W-S model is correct, that the mediator of the charged weak interactions, the W boson, has a mass between 50 and 150 $\mathrm{GeV/c}^2$, and the mediator of the neutral currents, the Z boson(s), is somewhat heavier. It must be emphasized strongly that this theory is not well proven. In fact it cannot be proven until we reach interactions where $Q^2 \gtrsim M_W{}^2$. High-energy e-p scattering is unlikely to produce the vector bosons directly, but surely will determine the dynamics of the weak interactions, from which we can infer their existence.

For the purposes of this study, we will accept the Weinberg-Salam model, and use it to calculate rates in e-p interactions.

2. Weak Neutral Currents. The neutral current in weak interactions have been observed in reactions of the type

$$\nu_\mu + Z \rightarrow \nu_\mu + \text{anything}$$

and

$$\bar{\nu}_\mu + Z \rightarrow \bar{\nu}_\mu + \text{anything}.$$

We anticipate that it should also contribute to the deep inelastic electron scattering

$$e + p \rightarrow e' + \text{anything}.$$

The rate due to the weak neutral current is very small, of order (relative to the electromagnetic interaction) $10^{-8}\ Q^4$ for $Q^2 \ll M_Z{}^2$. There is, however, a possibility of interference between the electromagnetic and the weak amplitudes. This would give a rate, again relative to the pure electromagnetic interaction, of order

$$10^{-4}\ Q^2\ (\text{GeV}/c^2) \text{ for } Q^2 \ll M_Z{}^2.$$

The detailed cross section formulae can be found in the excellent paper by Llewellyn-Smith and Wiik[1]. For our purposes, we note the following:

(i) There may be observable parity violation effects in ep→e+X. This is true even if no parity violation is observable in atomic-physics experiments where Q^2 is too small.

(ii) There may be observable charge-conjugation violation effects, much larger, and of different functional form than higher-order photon exchanges.

(iii) Even without the investigation of (i) and (ii) above (although they are to be desired), the effects on the total rate ep→e+X are observable, and are quite sensitive to the mass of the neutral vector boson(s).

Because of the nature of the system we are proposing, it seems unlikely that we can obtain significant polarization of the electron beam. (See Section X.A). Hence, parity-violation experiments, which involve comparing the rates for left and right handed incident

electrons are not within our grasp. In addition, we will not, at least in the early stages of operation, be able to fill the Main Ring with positrons. In view of these factors, we will consider only total rates for a beam of unpolarized electrons, and ignore the asymmetry experiments.

Figure III-10 shows the ratio for $e^-p \to e^-X$ total rate divided by the electromagnetic rate at x=0.15 and 0.25 as a function of y for Z masses of 85 GeV and infinity. It appears that the effect is large enough to be observed. Furthermore, the experiment is sensitive to the mass of Z with reasonable rates. Scaling violation might confuse the issue, since we are not measuring asymmetries. If asymptotic freedom theory is correct, we should be able to sort out the scaling violations at relatively low Q^2, where propagator effects are small, and observe the propagator effects at the larger Q^2, where scale violations have leveled off.

As an example of the power available from going to high S, Fig. III-11 shows the asymmetry in muon scattering in iron for 400 GeV muons. In this case, both polarizations are available in principle, and the luminosity is 10^3 higher. The effect is, however, so small that it is likely to be hidden by systematic errors. In addition, S is so low that the experiment is virtually insensitive to the Z mass.

3. Weak Charged Currents. The weak charged current cross section can be written as[1]

$$\frac{d\sigma}{dxdy}(ep \to \nu + X) = \frac{G_F^2 S}{2\pi}[(1-y)F_2 + y^2 x F_1 - y(1-y/2) \times F_3]. \quad \text{(III-4)}$$

We assume that the cross section for right-handed electrons vanishes identically, so in our unpolarized situation the luminosity is divided by two.

In many ways, this experiment is easier than that of detecting the neutral current, since we are looking for missing transverse momentum. If the apparatus is extended to small angles, the variables x and

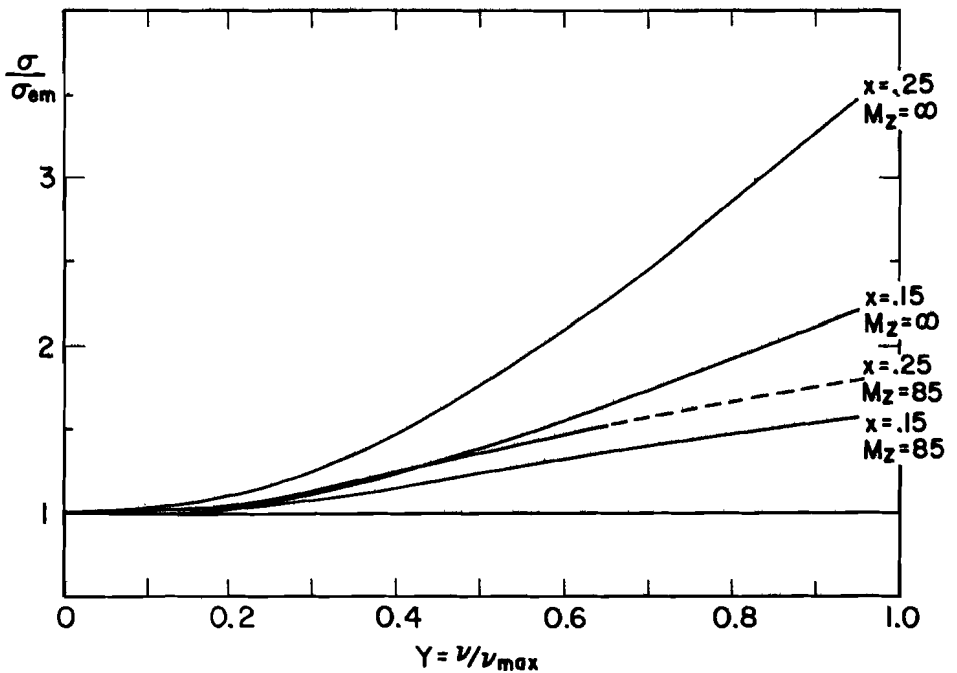

Fig. III-10. Ratio of the Total Cross-Section to e.m. for $e^-p \to e^-X$. S = 48000, M_Z = 85 GeV and ∞.

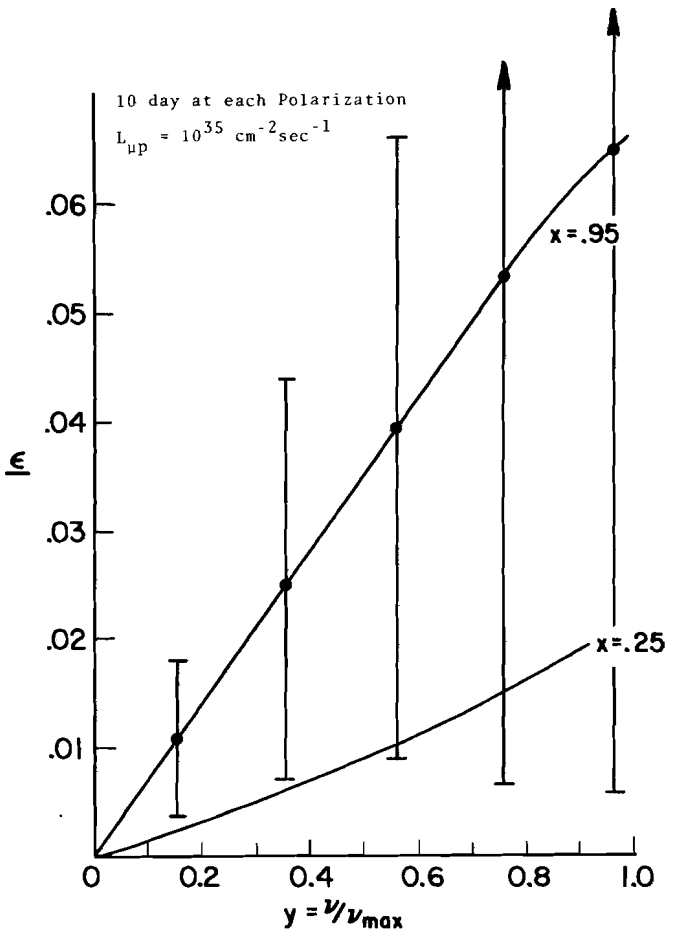

Fig. III-11. Asymmetry of μ-Scattering in Fe for 400 GeV Muons. Errors Are Statistical.

y can be reconstructed from the hadronic information. In other words, this would be equivalent to a narrow-band neutrino beam of energy 24 TeV. If x and y are known, the positron and energy of the lepton can be calculated. If it isn't there, it must have been a neutrino. If the parton model is taken literally, then θ_e and E_e' can be reconstructed even without knowledge of the forward hadronic final state. Figure III-12 shows the rate for events with $Q^2 > Q_o^2$ under the assumption of scaling for W masses of 75 GeV and infinity. Clearly, the events should be easy to see and should be sensitive to the W mass if the exact form of scale breaking can be determined from deep-inelastic scattering.

This experiment is one of the most important in high-energy physics. Short of direct observation of the W, there can be none with a higher priority.

E. The Detector

As mentioned previously, the detector design is dominated by the kinematics of e-p collisions, and only weakly influenced by the dynamics.

The experiment outlined in Sections II and III fall naturally into two classifications when one is considering detector design. They are:

(i) High Q^2 events such as deeply inelastic electron scattering or neutrino production, and

(ii) Low Q^2, low x events, such as electroproduction of flavors and diffractive photoproduciton of vector mesons.

Events of type (i) have the following features:

(a) An electron or neutrino comes backward at high energy and high transverse momentum.

(b) The transverse momentum of the lepton is balanced by the hadron system.

Because of the small angles of the recoil system and high energy it

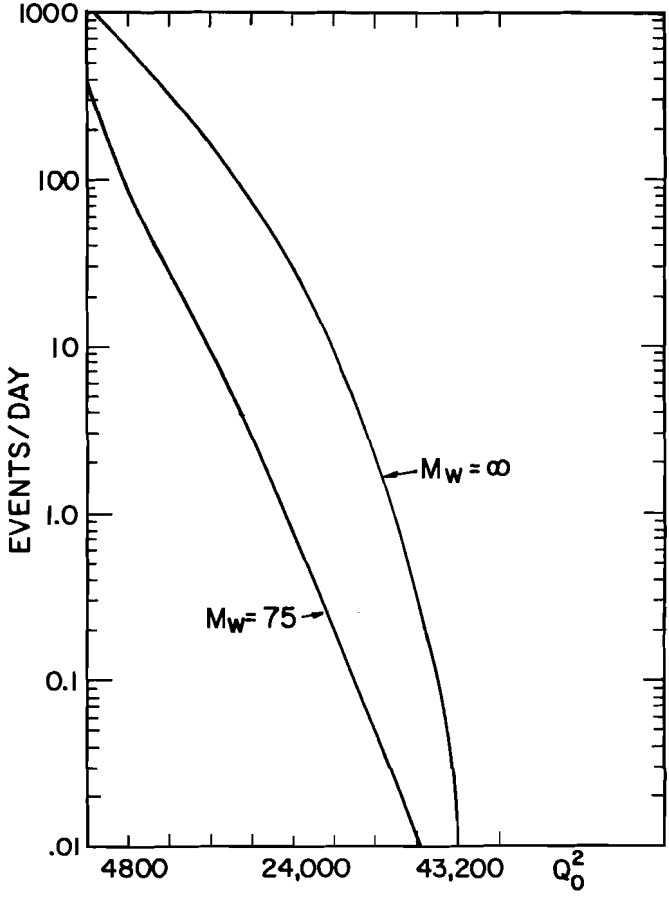

Fig. III-12. Events Rate with $Q^2 > Q_0{}^2$ for $e^-p \to \nu X$.

seems unlikely that one would gain any advantages with a solenoid or toroid magnet. A dipole magnet is eliminated because of the difficulty of running an electron beam through it. This leaves us with a detector which is totally calorimetric in the backward direction relative to the incident electron. For the inclusive electron scattering, one can trigger cleanly on P_t and E' of the electron, and since the electron has high energy, the resolution is very good. For the neutrino events, we put in logical "OR" a trigger based on P_t and E of the recoiling hadrons. Figure III-5 shows that triggering on P_t (hadron) > 10 GeV/c will cover all of the interesting region. Furthermore, a high P_t trigger eliminates most of the major hadronic background, which is beam gas scattering. The necessary part of the neutrino experiment is the ability to predict, from the hadronic information the approximate location recoiling lepton. In order to do this one must measure as much of the hadronic energy and P_t as possible, so the detector must have active calorimetry close to the beam. To accomplish this end, we instrument the faces of the quadrupoles and kissing magnets with calorimetry. In general, we would like to cover from a few milliradians out to about 90°. Hence, the end cap is strongly emphasized.

Events of type (ii) are at much lower energies and, on the whole, at much "larger" angles, some even in the forward hemisphere. In this region, calorimetry is not so effective and the particles can be analyzed much better with a solenoid magnet. In addition, one is more interested in a detailed analysis, including the effective mass reconstruction of events.

In the forward direction (for electrons) one might put lead glass or some other sort of shower counter for the tagging of electrons. This will give us a tagged photon beam for almost real photons: $Q^2 \sim 0$. Triggers might include looking for direct muons or multiple leptons from the decay of flavors, hidden or bare.

Figure III-13 is a kinematic polar diagram with labels as to what

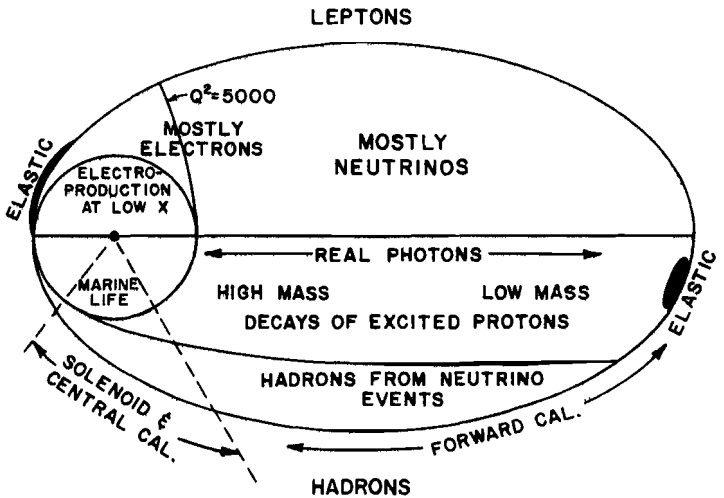

Fig. III-13. Willis Kinematic Polar Diagram.

happens in each region.[9] Using this, it is easy to design the optimum (for physics, not cost) detector. It is clear that each part of the detector stands alone. One might start with just the end cap, for example, or just the central calorimeter, and add the rest of the system later as the budget allows.

The calorimeters not associated with the magnet are straightforward; plexipop and lead for the electromagnetic showers, and plexipop and heavy concrete for the hadrons. It is basically the result of a study by the Fermilab Colliding Detector Group, in which an attempt was made to optimize a non-magnetic detector for p-p and $\bar{p}$-p collisions. Whereas it is not obvious in hadronic collisions that a non-magnetic detector is meaningful, it is quite clear in the e-p case that one does not need a magnet for the deep inelastic or neutrino events. A direct result of using electrons as a probe of hadrons instead of hadrons to probe other hadrons, is that it is very unlikely that one will build a detector that cannot do the physics we want. Even though we are sure to find many surprising results, we certainly have a much better idea of how to attack the problems of e-p scattering than the totally uncertain, and very model dependent predictions of p-p or $\bar{p}$-p collisions.

References (III)

1. C. H. Llewellyn-Smith and B. H. Wiik, Physics with Large Electron-Proton Colliding Rings, DESY 77/38, June, 1977.
2. "CHEEP, an ep Facility in the SPS", CHEEP Study Groups, Edited by J. Ellis, et al., CERN 78-02, Feb., 1978.
3. J. W. Humphrey and P. J. Limon, 1977 ISABELLE Summer Workshop, BNL 50721, p. 388.
4. D. Berley, et al., 1976 Aspen Summer Study, Vol. 1, p. 391, (Fermilab, 1976).
5. A. Abashian, et al., 1977 Aspen Summer Study, Vol. 2, p. 319, (Fermilab, 1976).

6. V. Barger and R. J. H. Phillips, Nucl. Phys. B73(1974), p. 269.

7. H. D. Politzer, Phys. Letters 70B, p. 430, (July, 1977).

8. R. P. Feynman, R. D. Field and G. C. Fox, CALT-68-595.

9. This representation is due to W. Willis, and was first presented at the ECFA Conference on ep colliding beams at Didcot, England, October, 1977.

IV. THE EXPERIMENTAL SET-UP

A. Generalities on the Detector

Because of the difference in triggering requirements, the detector for the neutrino reaction, $e^- + p \rightarrow \nu_e + x$, will be different from that for the deep-inelastic electron scattering, $e^- + p \rightarrow e' + x$. In the neutrino reaction, the signal is characterized by the lack of a scattered electron and by large transverse momentum of the final-state hadron jet. In the deep-inelastic electron scattering, the signal is provided by a very high energy electron in the backward hemisphere of the incident electron. Since the collision of 11.5 GeV x 1000 GeV is highly asymmetric in kinematics, most of the interesting particles will lie inside the forward hemisphere of the incident proton. The detectors can be made to cover only one side of the interaction region.

A non-magnetic detector appears to be most suitable for the neutrino reaction, while a magnetic detector is preferred for the deep-inelastic electron scattering. Furthermore, the following features should be preserved:

(i) No magnetic field in the vicinity of the interaction region. This will simplify greatly the pattern recognition task. In addition, the production angles, or the direction of the energy flow, can be determined with greater accuracy.

(ii) Split Detector and Flat Geometry:

for easy maintenance and construction, all the wire chambers will be made flat. All the detectors will be split into left and right sections. A gap will be left in the middle along the bending plane to let the intense bremsstrahlung through without interaction. There are difficulties involved in maintaining the equipment of colliding-beam experiment because of the general inaccessibility. A split detector will permit repair or replacement in the shortest possible time.

Based on ISR experience, 30~50% spare wire chambers are necessary. They should constantly be in a ready state to facilitate the expected replacement process.

B. The Non-Magnetic Detector

The non-magnetic detector for the reaction $e^{-}+p \rightarrow \nu_e+x$ is shown schematically in Figure IV-1. Basically, the system consists of two sets of drift chambers, two pairs of x- and y- hodoscopes, one lead-glass hodoscope, and one segmented hadron calorimeter. Each set of drift chambers contains six x- and six y- planes. The overall dimension of the active area is 3m x 3m. Each chamber will split into two halves as shown in Figure IV-2. This arrangement will make repair work easy. In addition, the two holes can accommodate the two beam pipes.

The lead-glass hodoscope is made of 34 x 34 pieces of lead-glass, each of dimension 3.5 in. x 3.5 in. x 14 in. (14 r.ℓ.). Its function is mainly to veto the deep-inelastic electron scattering events.

The two pairs of x- and y- hodoscopes are used to mask the tracks, and to form the triggers.

The segmented hadron calorimeter is made of 40 layers of 1-in. thick steel plates (8 collision lengths). Between each two layers of steel plates, there will be 10 x 10 pieces of scintillation counters made of NE114 scintillators. The calorimeter has an active area of 3m x 3m. Again, it will be split into two halves, along the vertical direction. Each scintillator will be split in such a manner that every scintillator in the device will have the same size, 0.3m x 0.3m x 1.5m. We believe that the grain size should be fine enough to allow P_T-selective triggers, but we may keep the option of reducing the grain size by a factor of two with a modest increase in cost.

C. The Magnetic Detector

A most versatile detector for the 11.5 GeV x 1000 GeV ep collision is a magnetic spectrometer as shown in Fig. IV-3. The magnet is a conventional toroidal magnet except that there are six air gaps. These air gaps allow the opportunity of doing magnetic analysis on the scattered electrons and final state charged hadrons. A specific design is shown

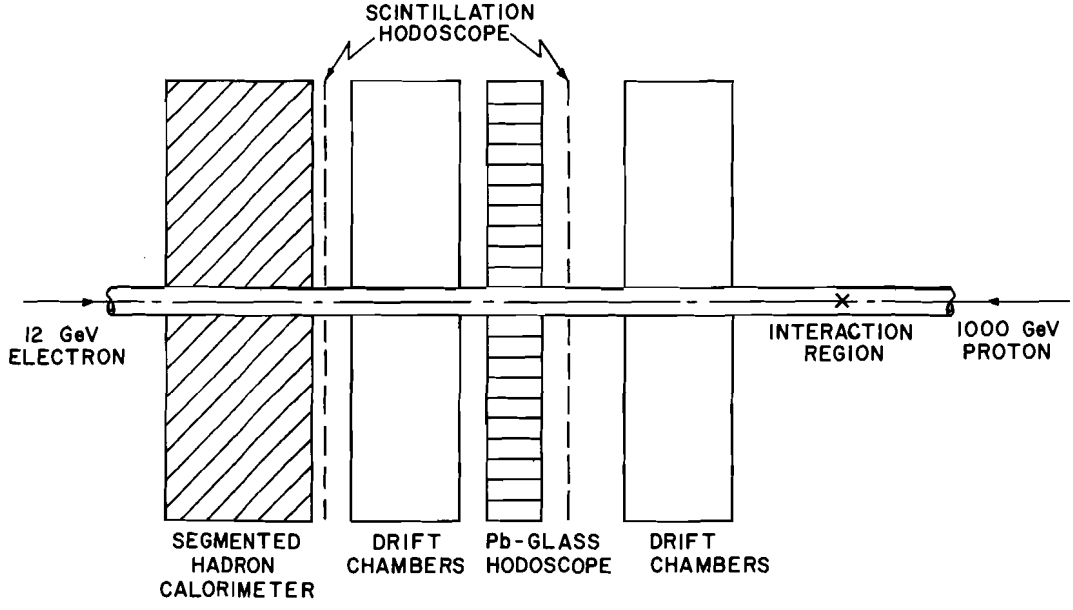

Fig. IV-1. Schematic Diagram of the Non-Magnetic Detector.

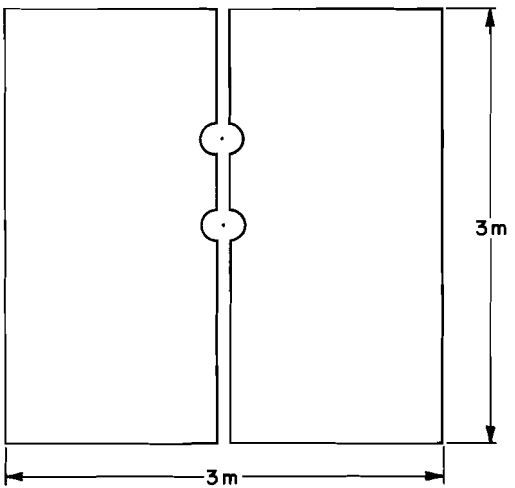

Fig. IV-2. Cross Section of the Drift Chambers.

in Figs. IV-4 and IV-5. The following characteristics of this spectrometer are noted:

(i) The magnet has a hole in the center to accommodate the beam pipes as well as to avoid high counting rates at small angles. The magnetic field can be completely shielded from the beam region lest it should interfere with beam operation.

(ii) The magnetic field varies as 1/r, where r is the radius. Since the magnetic field is transverse to the beam direction, it gives the best magnetic analysis power. Moreover, particles at small angles with respect to the proton direction, which usually have the highest momenta, will be subject to stronger magnetic bending.

(iii) The cylindrical symmetry of the magnetic field will greatly simplify track reconstruction. Since straight lines will be measured before and after the wheel-shaped magnet, their impact parameters along the radial direction and with respect to the magnet center can be easily determined. For straight lines belonging to the same particle track, their impact parameters in the radial plane should be equal because of angular-momentum conservation. For projections in the azimuthal direction, the tracks remain straight lines because there is no bending. This method offers an exceedingly simple algorithm to solve the complicated track-finding problem. It should be also kept in mind that this method does not require a "perfectly-shaped" magnetic field. All that is required is approximate cylindrical symmetry of the magnetic field. Most of the algorithm can be performed by specially designed high-speed microprocessors, instead of using pure software.

(iv) All the detector elements are split into two halves to facilitate maintenance and to avoid high-intensity bremsstrahlung in the bending plane.

As a general remark, we comment that both the magnetic and the non-magnetic spectrometer described here can easily fit into a space of approximately 5m after the interaction region. The transverse dimension of the enclosure has to be large enough to permit the removal of the detectors, particularly the wire chambers, for repair or replacement. We further comment that these spectrometers are also quite suitable for the study of lepton-pair production in pp collisions.

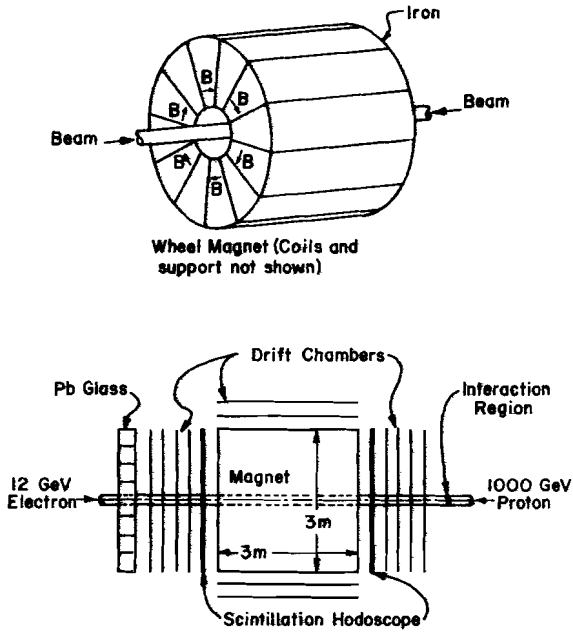

Fig. IV-3. Schematic of a Magnetic Spectrometer for the Reaction e+p → e'+hadrons in 12 GeVx1,000 GeV ep collisions.

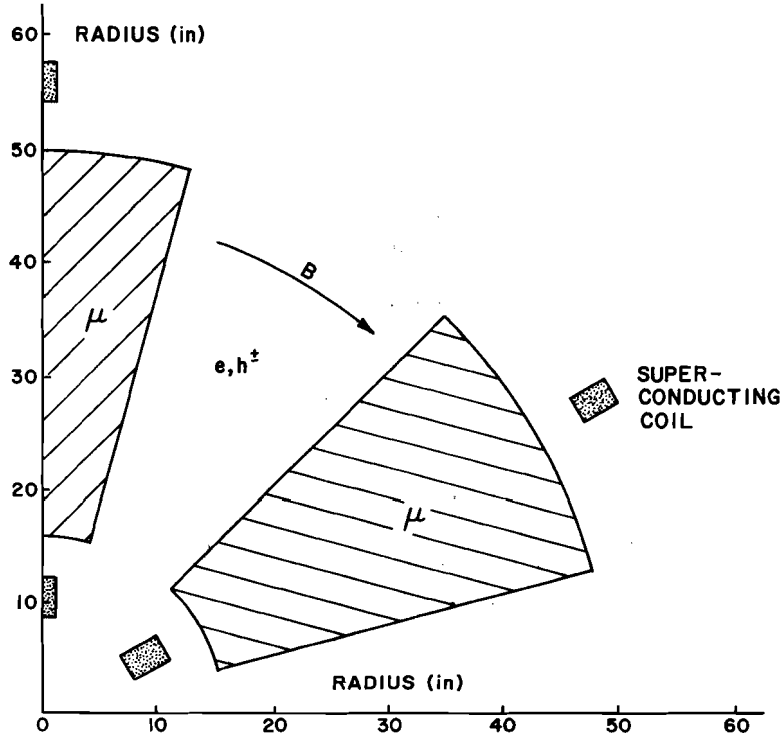

Fig. IV-4. Cross Section of Magnetic Detector.

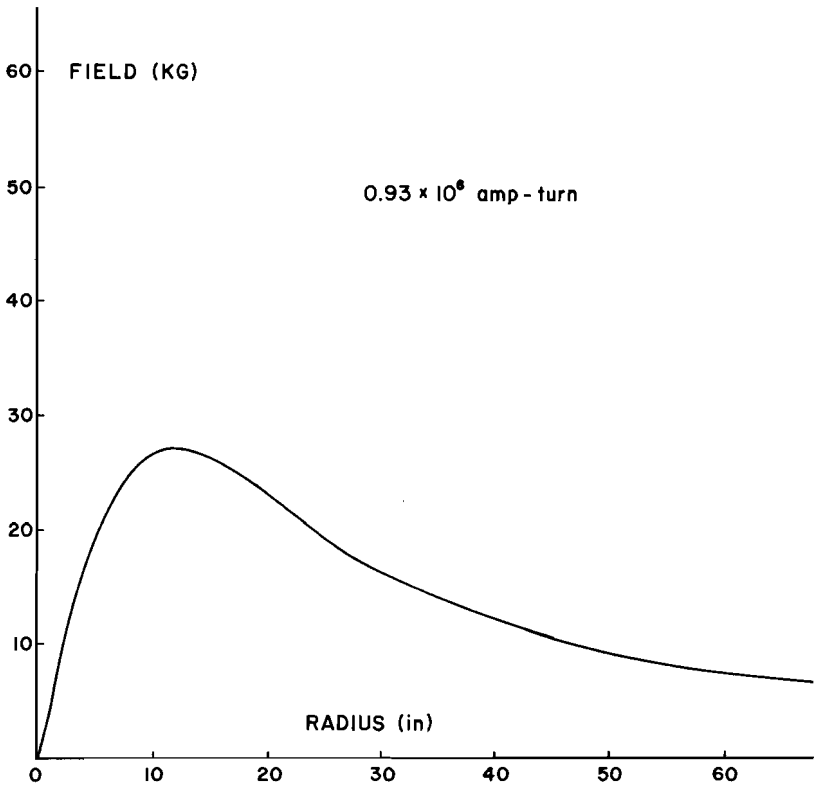

Fig. IV-5. Median Plane Air Gap Magnetic Field.

V. THE ELECTRON-BEAM SOURCE

A. The Electron Linac

The major requirement is either to build an electron linac or, more likely, have one built by a private company. In this case, we can specify the linac parameters to optimize injection and acceleration in the Cooling Ring. A set of desirable linac characteristics is given in Table V-1 below. The energy of 75 MeV corresponds to an injection field of 0.5 kG in the Cooling Ring and, as we shall see later, is large enough to avoid space-charge and intrabeam-scattering limitations. The linac could be operated in either L or S band. In either case, the frequency is considerably larger than 53 MHz, the value at which the beam is bunched in the Cooling Ring. A minimum repetition rate of 15 pulses per sec is desirable to match the Booster repetition rate. Each pulse should have a duration of 2μsec, which corresponds to four turns in the Cooling Ring and an average current within the pulse of 400 mA. If such current is not available, multiturn injection into the Cooling Ring is required. The beam emittance of 25π mm-mrad (for 95% of the beam) corresponds to single-turn injection. In case of lower linac current, smaller beam emittance would be required. For instance if the current is 100 mA, the total amount of 400 mA desired could be achieved with four-turn betatron stacking in the horizontal plane, provided the beam emittance out of the linac is 10π mm-mrad. This would match the acceptance of the Cooling Ring which is $25\pi \cdot 10^{-6}$ m-rad vertically and $40\pi \cdot 10^{-6}$ m-rad horizontally.[1]

The full energy spread of 1% (for 95% of the beam) is probably the maximum that can be accepted by the Cooling Ring.[1] This ring has momentum and betatron acceptances large enough to capture a rather large $\bar{p}$ beam; thus the requirements to handle such beam will insure the capability of the ring to capture the electron beam we have described.

Table V-1. Electron Linac Parameters

Output Energy	75 MeV
Frequency	$\geq$ 1 GHz
Repetition Rate	> 15 Hz
Pulse Length	2 μsec
Pulse Current	400 mA
Emittance	25π mm-mrad
Energy Spread (full)	1%

The search for a linac with these characteristics is still continuing. We are also asking the companies who build such linacs for cost estimates. A linac with beam specifications as shown in Table V-1 is in most respects a conventional one, very similar to models offered by private concerns. The energy-spread figure is perhaps somewhat small for 400 mA.

The linac will eventually be housed as close as possible to the Cooling Ring and properly radiation shielded. In addition, a power supply is needed for its operation. A chopper should be installed at the end of the linac to adjust the beam to the desired length.

The transport line between the linac and Cooling Ring has not yet been designed, but it does not seem to ba a major concern, provided it is made short enough to avoid space-charge blow-up during the transfer. Similarly, the location of the injection kicker has not yet been decided, because it is related to the siting of the linac itself.

B. Space-Charge Limit

At 75 MeV, the velocity of electrons is very close to c. Then in the limit $\gamma >> 1$ ($\beta \sim 1$) the space-charge limit is given by[2]

$$N = \frac{2\pi h^2 \gamma \nu \Delta\nu}{r_o R} ,$$

where N is the total number of particles in the ring, $\Delta\nu$ is the allowed shift in the number of betatron oscillations per turn ν, $r_o = 2.82 \times 10^{-15}$ m is the classical electron radius, R is the average radius of the ring, and h is the half height of the vacuum chamber. In the approximation that $\gamma >> 1$, this limit does not depend on the beam emittance and on

whether the beam is bunched or not.

The total number of electrons circulating at any time in either the Cooling Ring or the Booster is approximately 10^{12}. This beam will cause a tune shift of at most 0.01, which is quite small. On the other hand, the Main Ring, when completely full with 5×10^{13} electrons, exhibits a tune shift of 0.1 at 4 GeV and of 0.03 at 12 GeV. These tune shifts seem somewhat large, but theoretically there should already be a space-charge tune shift of approximately 0.1 for the usual proton beam circulating in the Main Ring at 8 GeV and such a shift does not seem to be of concern.

In any case, the space-charge limit does not occur in the Cooling Ring or the Booster, but rather in the Main Ring itself. The total of 5×10^{13} electrons is probably close to the limit, though we believe it is still on the safe side. With 1000 bunches in the Main Ring, the number of electrons per bunch is 5×10^{10}, which corresponds to an average current of about 400 mA, the current that our electron beam source will supply.

C. The Cooling Ring

1. The Magnet System. In the normal $\bar{p}$-mode, the Cooling Ring[1] operates at a constant momentum value of 644 MeV/c for cooling either protons or antiprotons. The nominal field of the bending magnets at this momentum is 4.5 kG. In addition, extremely good vacuum of the order of 10^{-10} torr is required to minimize beam-gas scattering and the consequent diffusion that could cancel the benefit of the electron cooling. To obtain such low pressure, it is necessary to have a metallic vacuum chamber inside the magnet bore. The vacuum chamber is made entirely of stainless steel and will not allow ramping of the magnetic field at too rapid a rate. If the Cooling Ring is also to be operated as an electron synchrotron, the magnetic field must ramp from an injection value of 0.5 kG (75 MeV/c) to the extraction level of 5 kG (750 MeV/c) in a reasonably short time to match, at least partially, the

Booster repetition rate of 15 cycles per second.

The limitation on ramp rate is caused by heating of the vacuum chamber by eddy currents. There is no water cooling. In Table V-2 we show the power dissipated and the temperature rise for different repetition rates, assuming synusoidal cycles between 0.5 and 5 kG.

Table V-2. Vacuum-Chamber Heating vs. Repetition Rate

Repet. Rate (sec^{-1})	Power Dissipated (kW)	ΔT (°C)
1	0.17	30
3	1.5	90
5	4	150
10	17	300
15	38	450

The temperature rise corresponds to the case in which all the power is dissipated in the stainless-steel vacuum chamber and is calculated for a total of 46 cycles required to fill the Main Ring.

We may conservatively conclude that the Cooling Ring can be operated safely with no water cooling of the beam pipe at a rate of three cycles per second. This will constitute one of our basic assumptions for further calculations. For instance, the Main-Ring filling time is affected by the Cooling-Ring repetition rate. Since the Cooling Ring and the Booster can accelerate only 24 bunches at one time and three batches each of 24 bunches are delivered to the Main Ring per second, the Main Ring will be completely filled in box-car fashion with 46 batches over a period of 15-1/3 seconds.

Eddy currents in the vacuum chamber due to ramping the field at three cycles per second cause a distortion of the bending field, primarily a sextupole component. At 1 in. from the center, the relative field error is estimated to be 2×10^{-4}, quite large, because it gives a contribution to the tune shift with momentum comparable to the natural chromaticity.

The Cooling Ring is a separated-function accelerator whose

lattice is shown in Fig. V-1 and applies to either cooling antiprotons or accelerating electrons. In the first mode, however, the quadrupoles are powered with six different power supplies, which may be too many to ramp in the electron-acceleration mode. Nevertheless, a solution can be found where the quadrupoles are divided into only two groups with two different excitations, which will be much easier to cycle. The resulting lattice, shown in Fig. V-2, is quite reasonable. Other parameters are shown in Table V-3. Thus a new power supply with three busses, one for the bending magnets and two for the quadrupoles, is required. A system of knife switches will select the right power supply for the desired operational mode of the ring.

Table V-3. Cooling-Ring Parameters for Electron Acceleration

Bending Field at inj. (75 MeV)		0.5 kG
Bending Field at extra. (750 MeV)		5.0 kG
Bending Radius (ρ)		5.0 m
Average Radius		21.56 m
Bending Magnet Length		1.3125 m
Quadrupole Length		0.6096 m
Quad Gradient at 750 MeV:	QF and QD	19.4 kG/m
	Q1F and Q1D	27.2 kG/m
Betatron Tunes:	ν_x	4.77
	ν_y	5.35
Chromaticity:	$\xi_x = \Delta\nu/(\Delta p/p)$	-9.12
	ξ_y	-11.79
Transition energy:	γ_T	3.77
Radiation Integrals:	$< G^2 >$	0.009251 m^{-2}
	$< G^3 >$	0.0018453 m^{-3}
	$< G^3 H >$	0.0028387 m^{-2}

Field measurements of both magnets have already been made and they give a good-field aperture ($\frac{\Delta B'}{B'} \sim 10^{-3}$ and $\Delta B/B \sim 10^{-4}$) at injection of 2 in. vertically and 5 in. horizontally, which corresponds to a vertical betatron acceptance of 25π mm-mrad and, after having subtracted 2 in. for the beam size caused by the momentum spread of 1%, to a horizontal betatron acceptance of 40π mm-mrad. The remanent field is small.

Moreover, the ring has sextupoles to achieve the desired chromaticity cancellation and widening of the momentum aperture to $\pm$ 1%. This aperture might seem large, but it is also required for the

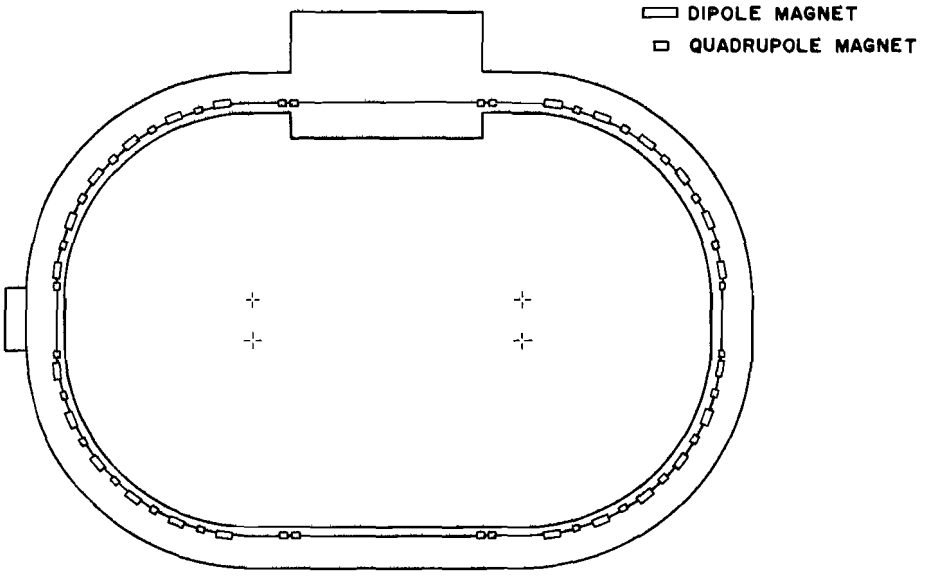

Fig. V-1. The Electron Cooling Ring.

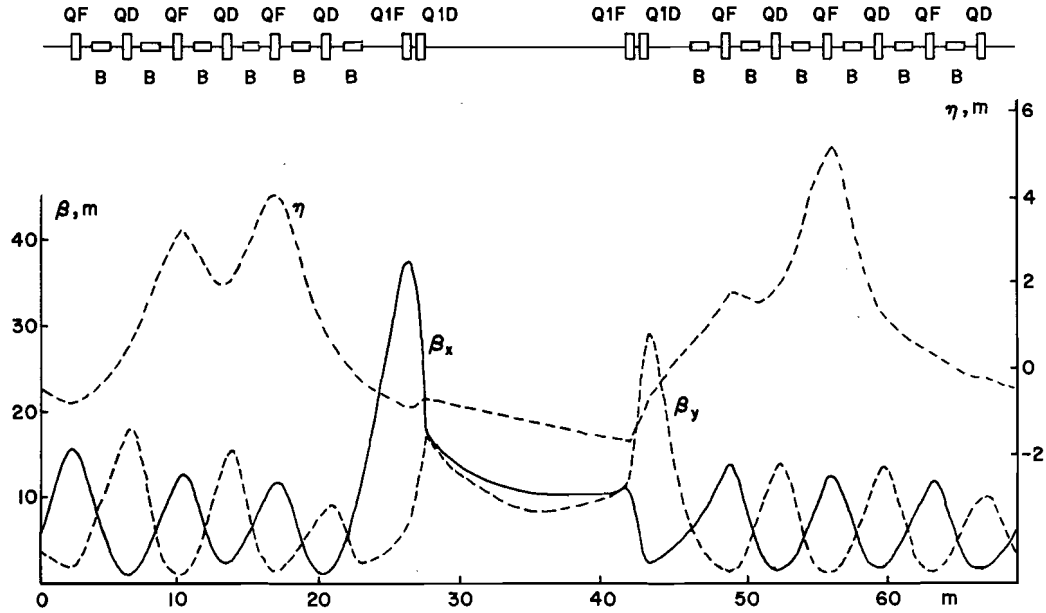

Fig. V-2. Modified Lattice of the ECR for the Acceleration of Electrons.

operation of electron cooling. Because the quadrupoles have different excitations, the sextupoles will also require different power-supply settings. These have not yet been calculated, but the power-supply system is flexible enough to accommodate any desired arrangement of excitations.

2. RF Acceleration. The velocity of the electrons is so close to the velocity of light that no frequency modulation is needed. We will use the rf systems presently available in the Booster and Main Ring and the natural choice for the accelerating frequency is therefore 53.105 MHz, which should apply also to the Cooling Ring. The circumference of the Cooling Ring is 3.5 times smaller than that of the Booster, with a revolution period of 0.452μsec. The rf harmonic number is then 24.

A pure sine-wave ramp at 3 Hz is rather expensive to realize and so we select a linear ramp like that shown in Fig. V-3.

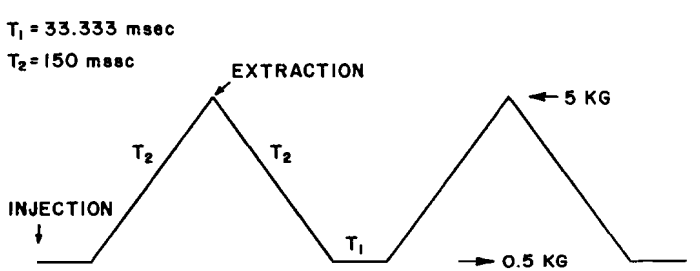

Fig. V-3. The Cooling-Ring Magnet Ramp

At injection, the energy lost to synchrotron radiation is only 0.6 eV per turn and it can therefore be neglected. Thus, for instance, if multiturn injection is required because of insufficient linac current, the stacking would be done using the same techniques used for proton beams.

The 400 mA will be injected at the beginning of a 33-msec front porch. Because of the large momentum bite (1%), the beam will completely debunch during the first few turns, and the high-frequency structure of the linac will be erased. The beam will be stable against self-bunching, provided the longitudinal coupling impedance Z/n is not larger than 1 kΩ. The phase-space area per rf wavelength (20 nsec) for a momentum bite of 1% is 0.015 eV-sec. The beam is adiabatically captured and bunched at the 24th harmonic during the 33 msec of the front porch. A final voltage of 40 kV per turn at the end of capture will provide rf buckets with areas of 0.025 eV-sec. It seems convenient to operate two rf cavities, each with 20 kV peak, at constant voltage and frequency. The required slow rise of the voltage seen by the beam for adiabatic capture can be accomplished by changing the relative phase of the two cavities. During acceleration, the only parameter needing adjustment will be the phase of the beam relative to the rf, which will be done by a radial-position loop.

The linear magnetic ramp corresponds to a constant energy gain of 2 keV/turn from 75 MeV to 750 MeV in 0.15 sec. Toward the end of the cycle, the electron energy becomes considerable and the radiation loss amounts to 5.6 keV/turn per electron. At this time, the energy gain required from the rf is 7.6 keV/turn. Denoting by ψ_s the synchronous phase angle, its dependence on beam energy is given by

$$\sin \psi_s = \frac{1}{20} + \frac{88.5}{80} E^4_{(GeV)}$$

The maximum power to be delivered to the beam occurs at the end of the cycle and is approximately 3 kW. A similar amount has to be delivered to excite the cavities.

The rf parameters are collected in Table V-4.

Table V-4. RF Parameters of the Cooling Ring

Beam intensity	400 mA
No. of electrons	1.13×10^{12}
Revolution frequency	2.213 MHz
Accelerating frequency (RF)	53.106 MHz
Harmonic Number	24
No. of Cavities	2
Total Voltage/turn	40 kV
Bunch Area at Injection	0.015 eV-sec
Momentum Spread at Injection	$\pm 0.5\%$
Bucket Area after RF Capture	0.025 eV-sec
Bucket Height after RF Capture ($\Delta E/E$)	$\pm 1.4\%$
Energy Gain/turn	2.0 keV
Energy Loss/turn at 750 MeV	5.6 keV
Bucket Area at 750 MeV	0.034 eV-sec
Bucket Height at 750 MeV ($\Delta E/E$)	$\pm 0.30\%$
Max. Power to the Beam (750 MeV)	3 kw
Total Cavities Shunt Impedance	1 MΩ
Power to the Cavities	1 kw
Max. Input Power Required (with 50% transmission efficiency)	8 kw
Synchronous Phase ψ_s: after RF capture	2.9°
at 750 MeV	23.6°
Phase-Oscillation frequency at 750 MeV	8.0 kHz

3. Radiation Loss and Beam Size at 750 MeV. Most of the radiation loss occurs toward the end of the acceleration cycle. As can be derived from Table V-4, the maximum power loss is 2.2 kW with a critical energy of 0.2 keV for the radiated photons. The average power, radiated over the entire acceleration cycle (1/3 sec) is only 225 W. Since there are 24 bending magnets, the average power radiated per magnet is at most 10 W, which is certainly small enough that it does not give any concern with either vacuum-chamber heating or with magnet radiation damage.

The Cooling Ring is a separated-function accelerator and therefore, the radiation reparation factors are[3]

$$J_H = 1 \qquad J_E = 2 \qquad J_V = 1$$

The damping time for the energy oscillations at 750 MeV is 60 msec, half that of the betatron oscillations. Thus we expect a significant contribution to the final beam size from radiation effects.

Three radiation integrals with which we calculate beam size

are shown in Table V-3. The quantity $\langle G^2 \rangle$ is the average of G^2 over one period of the accelerator. Here

$$G \approx 1/\rho$$

and

$$H = \gamma\eta^2 + 2\alpha\eta\eta + \beta\eta^2$$

are the lattice parameters.

Using a form developed by D. Edwards[4], the horizontal and vertical emittances at a time t during an acceleration cycle are given by

$$\varepsilon_H = 6\frac{\sigma_{H^2}}{\beta}\pi = \varepsilon_{Hi}\frac{E_i}{E}F(J_H,0,t) + $$
$$+ 6\pi C_q \frac{\langle G^3 H\rangle}{\langle G^2\rangle}\frac{E_f}{E}\frac{\gamma_f^2}{\tau_{of}}\int_0^t \left[\frac{E(t')}{E_f}\right]^6 F(J_H,t',t)\,dt' \quad \text{(V-1)}$$

and

$$\varepsilon_V = 6\pi\frac{\sigma_{V^2}}{\beta} = \varepsilon_{Vi}\frac{E_i}{E}F(J_V,0,t), \quad \text{(V-2)}$$

which is valid in the absence of coupling. In these equations, the indices "i" and "f" denote values at the beginning and end respectively of the acceleration cycle. Quantities without either of these two indices are evaluated at time t. In addition,

$$F(J,t't) = \exp\left(-\frac{J}{\tau_{of}}\int_{t'}^{t}\left[\frac{E(t')}{E_f}\right]^3 dt\right) \quad \text{(V-3)}$$

$C_q = 3.84 \times 10^{-13}$m, and τ_o is the characteristic time of the synchrotron radiation[3]

$$\tau_o = \frac{\text{E x revolution period}}{\text{energy loss per turn}}.$$

The second turn at the right-hand side of eq. (V-1) is the contribution from quantum fluctuations. The first term of eq. (V-1), and the right-hand side of (V-2) are the product of the inertial damping with the

radiation damping.

In our case, the energy increases linearly with the time and this gives, at 750 MeV,

$$\varepsilon_H = 0.05\ \varepsilon_{Hi} + 0.476\pi \text{ mm-mrad}$$

$$\varepsilon_V = 0.05\ \varepsilon_{Vi}$$

If the initial emittance is 25π mm-mrad in each plane, the final emittances are between 1 and 2π mm-mrad.

A similar expression for the rms energy spread at a time t during the acceleration cycle is[4]

$$\left(\frac{\sigma_E}{E}\right)^2 = \left(\frac{\sigma_E}{E}\right)_i^2 \frac{\Omega}{\Omega_i}\frac{E_i}{E}\ F(J_E,0,t) + $$
$$+ C_q \frac{\langle G^3\rangle}{\langle G^2\rangle}\frac{\Omega}{\Omega_f}\frac{E}{E_f}\frac{E_f^2}{E^2}\frac{\gamma_f^2}{\tau_{of}}\int_0^t \left[\frac{\Omega_f}{\Omega(t')}\frac{E(t')}{E_f}\right]^6 \times$$
$$\times\ F(J_E,t't)dt', \qquad \text{(V-4)}$$

where Ω is the angular phase-oscillation frequency. At 750 MeV,

$$\left(\frac{\sigma_E}{E}\right)^2 = 7.6 \times 10^{-3}\left(\frac{\sigma_E}{E}\right)_i^2 + 3 \times 10^{-8}$$

The contribution of the quantum fluctuations is small and can be neglected.

The longitudinal and transverse sizes of the beam extracted from the Cooling Ring are summarized in Table V-5.

Table V-5. Electron-Beam Parameters at 750 MeV

Horizontal Emittance	1.73π mm-mrad
Vertical Emittance	1.25π mm-mrad
Energy Spread (E/E, 95% of beam)	$\pm$ 8.5 x 10^{-4}
Bunch Length (95% of beam)	$\pm$ 36 cm
RF Bunch Area (95% of beam)	0.0024 eV-sec

They are relevant for acceleration in the Booster. The emittances are defined for 95% of the beam with biGaussian distribution and in the

absence of coupling. The initial emittance and energy spread are those of Table V-1.

The longitudinal emittance is probably too small because each bunch could hold 5×10^{10} electrons. The usual stability criterion,

$$|Z/n| \lesssim \frac{E/e}{I\ \gamma_T^2\ B} \left(\frac{\Delta E}{E}\right)^2, \tag{V-5}$$

where B(>1) is the bunching factor, gives a limit of 12 Ω for the impedance. This limit could be satisfactory for the Cooling Ring but not for the Booster, where the magnet laminations that are exposed directly to the beam would produce a larger impedance. Thus it seems the bunches will grow in the Booster; it is difficult to predict the amount of growth.

4. Touschek Lifetime. In an electron beam, elastic scattering of particles within a bunch cannot be ignored. Because of this scattering, the transverse momentum of a particle can suffer a reduction by an amount which then can be added to the longitudinal momentum. If the change is too large, the particle could be outside the momentum aperture and hence be lost. Even if the variations are small and not correlated, they can still cause a diffusion-like growth of the beam momentum spread. The loss rate due to this process is given by[5]

$$\frac{1}{\tau} = \frac{20.5\ r_o\ \gamma_T^2\ N_b\ f_\psi}{\varepsilon_x\ \delta_a^2\ \delta\ \gamma^3\ \sqrt{\varepsilon_y\ R/\nu_y}}\ C\left[\left(\frac{\delta_a}{\gamma}\right)^2 \left(\frac{6\pi R}{\nu_x \varepsilon_x}\right)\right], \tag{V-6}$$

where $r_o = 2.82 \times 10^{-15}$m, N_b is the number of electrons per bunch, f_ψ is the phase-oscillation frequency, $2\pi R$ the accelerator circumference, ν_x and ν_y are the number of betatron oscillations per turn, ε_x and ε_y are the betatron emittances (95% of the beam), δ is the rms relative energy spread in the beam, δ_a is half the relative momentum aperture, and C is a known function.[5] If $u \lesssim 0.01$, we can write

$$C(u) \sim \ln \frac{1}{1.78u} - \frac{3}{2} .$$

The Touschek Lifetime in the Cooling Ring from this formula is of the order of a few hours; in the Booster it ranges from 10 to 20 hours and in the MR is approximately 100 hours at 4 GeV and becomes practically infinite at 12 GeV. Thus the Touschek effect does not cause any concern. In contrast to other electron storage rings, the vertical emittance of the beam is always finite, and comparable in size to the horizontal emittance. This reduces the spatial density and the particles therefore rarely scatter on each other. Similarly, we are led to ignore the beam-size blowup due to the same process because it is insignificant.

This completes our consideration of acceleration of electrons in the Cooling Ring. The electrons would then be extracted and injected into the Booster following the pattern designed for the cooled antiproton beam.

References (V)

1. Design Report of the Fermilab Electron Cooling Experiment, Fermilab, Nov., 1977.
2. L. J. Laslett, Proc. 1963 Summer Study on Storage Rings, BNL 7534, p. 324, Brookhaven National Laboratory, New York.
3. M. Sands, SLAC-121, Stanford, November, 1970.
4. D. A. Edwards, Unpublished Note, Fermilab, 1975.
5. H. Brück, Circular Particle Accelerators, English translation, LA-TR-72-10 Rev., Los Alamos Scientific Laboratory (1972).

VI. ACCELERATION OF ELECTRONS IN THE BOOSTER

The Booster is more than adequate to capture a 750 MeV/c beam with the characteristics shown above in Table V-5, even if some bunch-area blowup should occur because of a longitudinal instability. It is well known from normal operation with protons[1,2] that betatron acceptance of the Booster is in excess of 20π mm-mrad in both planes and that the rf system is capable of capturing a beam with a full momentum bite over 0.5%.

The Booster[3] is also a rapid-cycling accelerator with a repetition rate of 15 Hz. The field excitation is of the form

$$B = \frac{1}{2}(B_f+B_i) - \frac{1}{2}(B_f-B_i)\cos 30\pi t \qquad \text{(VI-1)}$$

Normally the injection value corresponds to a momentum of 644 MeV/c. Thus the 24 bunches extracted from the Cooling Ring are transferred on the fly during the field rise to the Booster, at a later time than usual. The Booster already has the capability of having its injection time adjusted. The 24 bunches will be captured by existing rf buckets. The rf system will, of course, be operated at the constant frequency of 53.105 MHz, which corresponds to the usual harmonic number of 84. Only 24 of the 84 buckets will be occupied by beam.

The Booster will operate at its usual repetition rate of 15 Hz, while the Cooling Ring will operate at 3 Hz. Each cycle, which accelerates 24 electron bunches, will be followed by four cycles with no beam.

Bench measurements[4] have shown that it is possible to operate the Booster rf cavities at constant maximum frequency for a period of time that corresponds to the time required to fill the Main Ring. The bias current required is large, 2.1 kA, but it is not believed to cause any difficulties. The total voltage per turn available with 18 cavities is approximately 1.2 MV. Our plan is to run the cavities at constant peak voltage and to adjust their relative phases for the required energy gain

and for compensation of the synchrotron radiation losses.

The beam is already tightly bunched at injection and small in size compared with the rf buckets. A phase-lock system would be a convenient system for the synchronous transfer of bunches from the Cooling Ring to the Booster. The rf phase could be automatically adjusted with a beam radial-position loop. Observe that because of the large energy, the acceleration is all well above the transition energy (which, incidentally, is also true in the Cooling Ring and Main Ring), eliminating the rf phase-switching operation that is needed for a proton beam.

The Booster[3] is a combined-function accelerator made of two kinds of bending magnets with opposite gradient and slightly different bending radii. Relevant Booster parameters are shown in Table VI-1. The energy loss per turn is given by

$$U = 2.00 \times E_{GeV}^4 \quad \text{keV/turn} \qquad \text{(VI-2)}$$

The radiation repartition factors are anomalous. As expected, the radial betatron oscillations are anti-damped, but at twice the rate of other conventional electron-synchrotrons.[5] To minimize the radial-emittance increase, it will be advantageous to ramp the magnets in the usual proton cycle, from 200 MeV to 8 GeV proton kinetic energy and extract the 24 electron bunches on the fly when they have reached 4 GeV. At this energy, the radiation losses are already somewhat large, approximately 0.5 MV/turn, for compensation with the available rf voltage. The energy of 4 GeV is reached in 15 msec. The beam emittances may be calculated by means of eqs. (V-1) and (V-2) with the cycle specified by eq. VI-1.

We obtain

$$\varepsilon_H = 0.30\varepsilon_{Hi} + 0.20\pi \text{ mm-mrad}$$

$$\varepsilon_V = 0.15\varepsilon_{Vi}$$

Table VI-1. Booster Parameters

F-magnet:	B'/B	2.204 m^{-1}
	Length	2.92 m
	Bending Radius	41.211 m
D-magnet:	B'/B	-2.767 m^{-1}
	Length	2.92
	Bending Radius	48.488 m
Circumference		474.2 m
Betatron Tunes		$\nu_x = 6.7 \quad \nu_y = 6.8$
Transition Energy		$\gamma_T = 5.5$
Betatron Aperture		$\gtrsim 20\pi\ 10^{-6}$ m
Momentum Aperture ($\Delta P/P$)		~ 0.5% (full)
Repartition Factors		$J_H = -2.0$
		$J_E = 5.0$
		$J_V = 1.0$
Radiation Integrals		$\langle G^2 \rangle = 0.00030\ m^{-2}$
		$\langle G^3 \rangle = 6.8 \times 10^{-6}\ m^{-3}$
		$\langle G^3 H \rangle = 2.7 \times 10^{-6}\ m^{-2}$
Injection Energy		750 MeV
Extraction Energy		4 GeV
RF Frequency		53.105 MHz
RF Voltage		1.2 MV/turn
Revolution Period		1.58μsec
Harmonic Number		84
Emittance (4 GeV, 95% of beam)		0.5π mm-mrad

Insertion of the initial emittances from Table V-5 gives

$$\varepsilon_H = 0.72\pi \text{ mm-mrad and } \varepsilon_V = 0.19\pi \text{ mm-mrad}$$

These values are defined for 95% of the beam, assuming a biGaussian distribution, and are reasonably small. It is likely that the linear and nonlinear coupling in the Booster will equalize the emittances at approximately the common value of 0.5π mm-mrad. Similar calculations for a ramp up to 4 GeV in 33 msec with extraction at the top gives estimated emittances in excess of 2π mm-mrad, too large to be accepted by the Main Ring.

Correspondingly to eq. (VI-1), the assumed energy ramp is

$$E = \frac{1}{2}(E_f+E_i) - \frac{1}{2}(E_f+E_i)\cos 30\pi t,$$

with $E_i = 0.75$ GeV and $E_f = 8.89$ GeV. The energy gain per turn to fit this ramp is then

$$\Delta E = (606 \text{ keV/turn}) \sin 30\pi t$$

With the energy loss of eq. (VI-2), the synchronous phase must be programmed according to

$$\sin\psi_s = 0.505 \sin 30\pi t + 0.00167\, E_{GeV}^4$$

At 4 GeV ($t = 14.515$ msec), this gives $\psi_s = 67.12°$. Thus the voltage required is quite large at higher energies. If the actual 18-cavity system cannot deliver 1.2 MV, either more cavities will be added or the ramp is set for lower maximum field to ease the requirement on energy gain per turn, although this will be at the cost of increasing the radial betatron emittance. In this mode of operation, the bunch shape extracted from the Cooling Ring is not matched to the shape of the Booster rf buckets. The bunches are longer and narrower and will tumble. The tumbling will smear out because of nonlinearities and synchrotron-radiation effects. The tumbling will preserve the bunch length, but

will blow up the momentum spread. The increase is significant (a factor of 4.5) and has the positive effect that it raises the impedance limit as calculated according to eq. (V-5) to around 250Ω. The rf buckets are adequately large at all times to accommodate the beam bunches.

The beam energy spread at 4 GeV can be calculated from eq. (V-4). It is

$$\left(\frac{\sigma_E}{E}\right)^2 = 0.015 \left(\frac{\sigma_E}{E}\right)_i^2 + 0.3 \times 10^{-8}$$

which gives a rather small momentum bite that can be easily captured by the Main Ring. The bunch and bucket parameters are listed in Table VI-2.

Table VI-2. Booster Bunch and Bucket Parameters

Energy	0.75 GeV	4 GeV
ψ_s	0.03°	67.12°
Bucket Area	0.344 eV-sec	0.024 eV-sec
Bucket Height	$\pm 1.9 \times 10^{-2}$	$\pm 0.12 \times 10^{-2}$
Bucket Length*	±36 cm	±17.4 cm
Energy Spread*	$\pm 3.8 \times 10^{-3}$	$\pm 5 \times 10^{-4}$
Phase Oscill. Freq.	16.8 kHz	4.54 kHz

*95% of the beam

The above calculations apply to the motion of an electron that moves close to the main orbit. Because of the magnet gradient, different emittance values are expected for particles with different momenta. This problem is not believed to be serious.[6]

The Booster is already equipped with sextupoles for chromaticity compensation during the ramp. It is also provided with radial and vertical dampers, so that we do not expect collective instabilities that cannot be handled.

Since there will be no more than 24 bunches at any time, the average current is 110 mA, and the total power radiated at 4 GeV is 56 kW, quite small. There are 46 magnets and a peak of 600 W will therefore be

deposited in each magnet. At this peak, the critical radiation energy is approximately 4 keV. The total average power is only about 1 kW, about 10 W/magnet. The Booster does not have a vacuum chamber to shield the laminations and the coils from radiation, but the coils are 2 in. above and below the median plane where the radiation is concentrated, so the radiation striking the coils is small. We do not expect any radiation damage to the laminations, and the heating caused by the power loss will be very small.

Our study shows that acceleration of electrons in the Booster is indeed quite possible and that the modifications required for this mode of operation are trivial. When acceleration is completed, the electron beam is extracted on the fly and transferred to the Main Ring through the same transport line that is planned for the antiproton beam.

References (VI)

1. E. R. Gray, et al., Proc. of the 1975 Particle Accelerator Conference, Washington, March, 1975, p. 1897.
2. E. R. Gray, et al., Proc. of the 1975 Particle Accelerator Conference, Washington, March, 1975, p. 1901.
3. Booster Synchrotron, TM-405, Jan., 1973, edited by E. L. Hubbard.
4. J. Bridges, private communication, Spring, 1978.
5. D. A. Edwards, Unpublished Note, Fermilab, 1975.
6. D. A. Edwards, TM-566, Fermilab, April, 1975.

VII. ACCELERATION AND STACKING OF PROTONS IN THE ENERGY DOUBLER

A. The Proton Beam Characteristics

The acceleration and stacking of protons in the Energy Doubler have already been investigated in connection with the Fermilab pp and $\bar{p}p$ colliding-beams projects.[1] We know what we may reasonably expect for the characteristics of a 1000-GeV beam. Moreover, the proton beam originates from the Main Ring and the performance of that accelerator is well established.

For our scheme, as well as for the other projects, the intensity required is 2×10^{13} protons per pulse from the Main Ring. Attainment of such intensity is now routine and we know that it is associated with an emittance of $1.5\pi \cdot 10^{-6}$ m-rad in each plane at 8 GeV (including 95% of the beam and assuming a biGaussian distribution).[2] In studies of beam storage,[3] it was determined that the beam emittance increases linearly with time, the rate of increase being roughly inversely proportional to the second power of the energy. It is suspected that such blowup is caused by a combination of multiple Coulomb scattering with the residual gas, nuclear scattering, and irregularities of the guide field. Gas scattering is the most important effect because of the poor vacuum in the Main Ring which at the present is in the 10^{-8} torr range. The beam lifetime is also affected by these processes; it increases with the square of the energy and is of the order of a few hours at 200 GeV.

The Energy Doubler will perform better, first because the vacuum pressure will be at least an order of magnitude lower and second because of the large beam energy (1000 GeV). We can expect little dilution of the beam emittance, which we can scale with momentum from its value at 8 GeV. The lifetime will also be long enough that refilling of the Energy Doubler can occur once or at most twice a day without the beam deterioration becoming too appreciable.

RF stacking of ten or more pulses in the Energy Doubler at 100 GeV has also been investigated[4] and it seems quite feasible for reasonably

good magnet quality, chromaticity cancellation and a wide-enough momentum aperture (±0.35%). Thus a final current of 1.5A, corresponding to 2×10^{14} protons, looks attainable.

B. Longitudinal Stability and Bunch Area

One beam parameter that is not well determined is the longitudinal bunch area. There are indications that at very low energies (below transition energy), this area is not larger than 0.1 eV-sec per bunch, five times the design value. At higher energies, greater than approximately 100 GeV, a bunch-lengthening phenomenon has been observed which might be induced first by coherent dipole oscillations and then by the smearing processes of the nonlinear accelerating forces. The lengthening, if accompanied by widening in momentum spread, would lead to a growth of the bunch area to more than 0.3 eV-sec. This occurs for an intensity of 1.5×10^{13} protons per pulse. The current dependence has not been definitely determined yet, but something like a threshold effect has been determined by enhancing the bunch-area increase in a controlled way with the bunch spreader.[5] It was found that if the initial bunch area is 0.23 eV-sec or larger, lengthening does not occur at the higher energies.

Although these observations require confirmation and clarification, a longitudinal bunch instability is nevertheless expected for large currents at large energies. From the usual stability criterion (V-5) (which is actually valid for a coasting beam,[6] but can also be applied *ad hoc* to a bunched beam[7,8]) we derive a value of 35Ω at 100 GeV for the impedance Z/n. During the formation of the stack, because of imperfect stacking efficiency, the ratio $(\Delta E/E)^2/IB$ in the right-hand side of eq. (V-5) increases and larger impedance values can be tolerated. This effect is partially cancelled by the energy increase between the stacking period and the end of the acceleration. Assuming also that the Energy Doubler has the same impedance, 35Ω would set a limit on the bunch area at 1000 GeV for a 10-turn stacking (intensity of 1.5A) of not

less than 4 eV-sec. It has been estimated that this is also approximately the bunch area one could expect from rf-stacking considerations. The parameters shown in Table II-1 have been based on all these considerations.

One might consider initially performing a preliminary ep experiment at lower luminosity without attempting, for instance, rf stacking in the Energy Doubler, but employing only one pulse for the Main Ring. The stability considerations are the same as those discussed above, and for the same rf voltage per turn, 1MV, lead to a bunch-area stability limit of 0.9 eV-sec at 1000 GeV. This could be achieved by blowing up the beam in a controlled fashion with a bunch spreader at lower energy in the Energy Doubler. Because of the relatively large crossing angle, the luminosity is proportional to proton-beam current and inversely proportional to the bunch length. There is therefore only a variation of a factor 3 between the two cases of rf stacking and single turn.

C. Other Instabilities

The Main Ring has been operated for long periods of time at energies over 100 GeV with up to 2×10^{10} protons per bunch without exhibiting crucial collective instabilities. Transverse coherent instabilities[9] are damped by means of two sets of electronic feedback circuits over a large frequency range, including individual bunch modes. Of course, only dipole oscillations are corrected but we do not have any indication of higher internal modes at the present current and energy levels.

Bunch-to-bunch longitudinal instabilities[10] have been partially damped down to a level that is compatible with the normal mode of operation by reducing the shunt impedance of parasitic modes in the rf cavities. One might believe that they are ultimately responsible for the bunch dilution observed in the storage mode at 100 GeV. We do not have clear-cut evidences of higher internal bunch-to-bunch modes.

In our scheme, we need to operate the Energy Doubler at larger

energy and with ten times as many protons per bunch. Obviously, there is some concern about the stability of this higher-intensity beam. It is likely the Energy Doubler also will be provided with sets of electronic dampers to control transverse instabilities and care will be taken to eliminate parasitic modes in the rf system. We believe that dipole oscillations of either kind can be eliminated, but we are concerned about the enhancement of higher modes of oscillations which are harder to observe and to control. We have not investigated this point further; it is also a concern to the other colliding-beams experiments (pp and $p\bar{p}$) where higher intensity is required. These effects will require a deeper analysis.

References (VII)

1. Fermilab TeV Program, Superconducting Magnet Ring, Fermilab, 1977.
2. R. Diebold, Proceedings of the 1977 Aspen Summer Study on Colliding Beam Physics at Fermilab, Vol. 1, p. 83.
3. A. V. Tollestrup, Proc. of the 1977 Aspen Summer Study on Colliding Beam Physics at Fermilab, Vol. 1, p. 97.
4. A. G. Ruggiero, TM-272, Fermilab, April, 1977.
5. S. Ecklund, Proc. of the 1977 Aspen Summer Study on Colliding Beam Physics at Fermilab, Vol. 1, p. 147.
6. E. Keil and W. Schnell, CERN-TH-RF, 69/48 (1969).
7. D. Boussard, CERN, Lab 11/RF/Int. 75-2 (1975).
8. H. Hereward, Proc. of the 1975 ISABELLE Summer Study, July 1975, Brookhaven, N. Y., Vol. II, p. 555.
9. R. Stiening and E. J. N. Wilson, Proc. of IX Intern. Conference on High Energy Accelerators, Stanford, 1974, p. 329.
10. R. F. Stiening and J. E. Griffin, Proc. of the 1975 Particle Accelerator Conference, Washington, p. 1859.

VIII. ACCELERATION AND STORAGE OF ELECTRONS IN THE MAIN RING

A. The Collision Region and the Main-Ring Lattice

The electron beam size depends on both the Main Ring lattice and the synchrotron radiation effects. Since the collision region affects the Main Ring lattice very strongly, we begin this section by discussing it.

The colliding region is symmetric around the crossing point; half of it is shown in Fig. VIII-1. When the Energy Doubler is installed under the Main Ring, the two beam axes will be separated vertically by 25 in. It is easier to bend the electron beam, because of its lower momentum, and bring it down to the elevation of the proton beam. This is accomplished with four 4-m long vertical bending magnets. Two of these are located at the end of one long straight section and the other two are located about 10 m away from the crossing center. These latter magnets, as well as the quadrupoles next to them toward the center, are shared by both beams. Although the effect on the proton beam is relatively small, the dipoles are compensated by two more, installed on each side of the Energy Doubler long straight section. The effects of the quadrupoles shared by both beams will be compensated by resetting some of the other quadrupoles in the low-beta insertion for the Energy Doubler.

The low-beta insertion in the Main Ring is shown in Fig. VIII-2. The beta value at the crossing point is approximately 30 cm and the dispersion function at this point is kept very small. The insertion is antisymmetric and five additional independent power supplies are required to energize the regular quadrupoles. These will be set at higher excitation than usual to give a larger betatron tune in order to reduce the electron beam emittance. The Main-Ring lattice parameters are shown in Table VIII-1.

The low-beta insertion is not properly matched with regard to both beta and dispersion functions. The mismatch occurs in both planes but

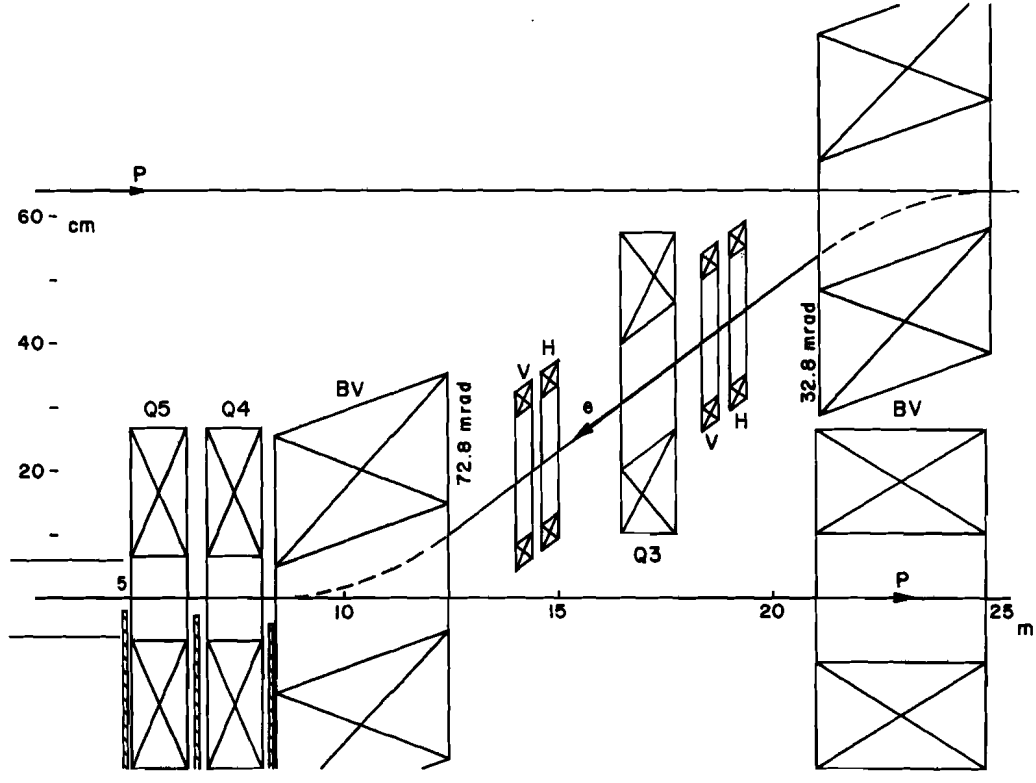

Fig. VIII-1. Half of the e-p Colliding Region.

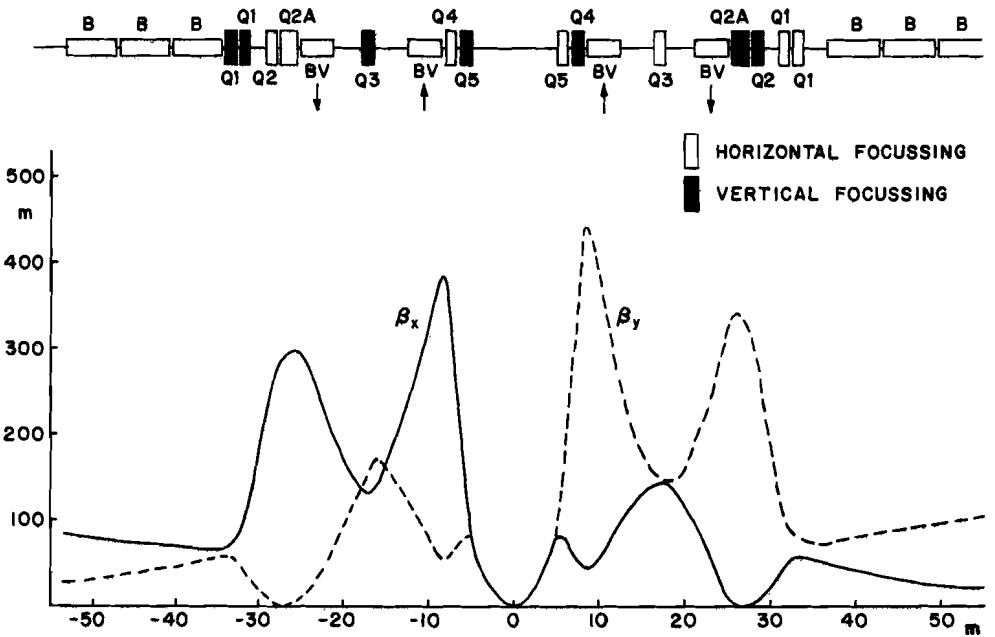

Fig. VIII-2. Low-Beta Insertion for the Main Ring.

Table VIII-1. Main-Ring Lattice Parameters with Low-Beta Insertion

$B\rho$ (12 GeV):		400 kG m
Average Radius:		1000 m
Regular Dipoles, (B):	total number	774
	length (ℓ)	6.0706 m
	bending radius (ρ)	747.8125 m
Vertical Dipoles, (BV):	total number	4
	length	4 m
	bending radius	80 m
	field	5 kG
Regular Quads:	gradient, Hor. Foc.	9.180 kG/m
	, Vert. Foc.	9.173 kG/m
Insertion Quad:	length	4 ft
	gradient: Q1	34.61 kG/m
	Q2	19.47
	Q2A (7' long)	19.47
	Q3	48.23
	Q4	112.92
	Q5	122.89
Transition Energy (γ_T):		24.1054
Betatron Tunes:	ν_x	26.72
	ν_y	26.67
β^*		35 cm (hor), 30 cm (vert)
η^*		1 cm (hor), -6 cm (vert)
β_{max}, insertion		380 m (hor), 438 m (vert)
β_{max}, reg. lattice:	horiz.	165 m
	vert.	210 m
η_{max}, reg. lattice:	horiz.	6.0 m
	vert.	0.8 m

is more pronounced in the vertical, where wiggles on the dispersion with amplitude 0.8 m and on the beta function with a total maximum up to 210 m are added. This by no means represents the best insertion, but it is a workable one. Full matching can be obtained by exciting the quadrupoles at symmetric locations around the crossing point with different power supplies.

The vertical dipoles are rotated around their axes by the small angle indicated in Fig. VIII-1 to set the trajectory of the electron bunches at a horizontal crossing angle of 2 mrad with the proton trajectory. The direction of rotation is opposite on the two sides of the crossing point.

B. Filling of the Two Rings

The best procedure for filling the two rings is thought to be the following:

(i) During acceleration of protons to 100 GeV, the Main Ring is operated as usual, with no low-beta insertion and at nominal betatron tunes. The vertical dipoles are not powered and the trajectory of the protons is the straight line shown in Fig. VIII-1.

(ii) The proton beam is transferred to the Energy Doubler, where it is eventually stored with other pulses. During this operation, the Energy Doubler is also operated at the nominal tune. The low-beta insertion is not activated and, in particular, the quadrupoles near to the crossing region are not used.

(iii) The same mode of operation applies during acceleration to 1000 GeV in the Energy Doubler.

(iv) At the end of the acceleration cycle, the Energy Doubler is switched to the storage mode of operation. The low-beta insertion is activated, including the quadrupoles which are shared by both beams.

(v) Before electrons are injected in the Main Ring, the six vertical dipoles are ramped to their value for beam-crossing operation. The Main Ring tune is also switched to a higher value. Finally, the Main Ring low-beta insertion itself is activated.

(vi) The 4-GeV beam is injected into the Main Ring, already operating in the storage mode. Care will be taken to avoid having the two beams collide with each other during the acceleration. This can be accomplished by dephasing the rf cavities of the two rings.

(vii) Once the Main Ring has been filled, the electron beam is accelerated to 12 GeV, where then it is made to collide with the proton beam. Thus at injection, the Main Ring is already operated with the low-beta insertion on and the electrons go through the vertical bend at the interaction region.

C. Synchrotron Radiation and Electron-Beam Parameters

The Main Ring is a separated-function accelerator with straight (non-wedged) dipole magnets. Along the orbit that goes through the axis of the quadrupoles, the radiation repartition factors are given by

$$J_H = 1, \; J_V = 1, \; J_E = 2.$$

Combining the effects of the regular horizontal dipoles with the four vertical ones discussed in Section VIII.A above and taking into account the low-beta insertion in the lattice, one has the following radiation integrals

$$\langle G^2 \rangle = 1.7 \times 10^{-6} \; m^{-2}$$
$$\langle G^3 \rangle = 6.8 \times 10^{-9} \; m^{-3}$$
$$\langle G^3 H \rangle = 2.9 \times 10^{-10} \; m^{-2}$$

From these integrals we calculate the following relations of emittances to the beam energy E

$$U = 0.15 \; E^4_{(GeV)} \; \text{keV/turn}$$
$$\varepsilon_H = 0.0015 \cdot \pi \; E^2_{(GeV)} \; 10^{-6} \; \text{m-rad}$$
$$\varepsilon_V = 0.0032 \cdot \pi \; E^2_{(GeV)} \; 10^{-6} \; \text{m-rad}$$
$$\sigma_E/E = 5.355 \times 10^{-5} \; E_{(GeV)}$$

These quantities are calculated at equilibrium with the synchrotron

radiation. U is the total energy loss per turn; about one-fifth of this is due to the four vertical bending magnets in the crossing region, which appears to be a serious limitation. A scheme with more than one crossing is not possible without adding more rf voltage and power, by adding additional rf stations. The emittances ε_H and ε_V are again given for 95% of the beam particles; if σ denotes the rms beam size,

$$\varepsilon = 6\pi\frac{\sigma^2}{\beta} .$$

It may be noted that the vertical emittance is about twice the horizontal. This increase is caused mainly by the low-beta insertion and the vertical bending magnets and partially by the lattice perturbation caused by the insertion mismatch.* The quadrupole setting described in Section VIII.A gives a reasonably small value for ε_H, but this value depends quite strongly on the quadrupole strength; a minor change of it could cause a considerable increase in the mismatch and hence a doubling or more of the horizontal emittance, whereas the vertical emittance will remain practically unchanged. The use of ten power supplies, rather than five, to achieve the desired low-beta value can considerably reduce the mismatch and provide a more efficient mode of operation with better control of the beam emittance.

Finally, σ_E/E is the relative rms energy spread. The contribution to σ_E from the four vertical bending magnets is quite large (almost a factor of two).

The total voltage the Main-Ring RF system can produce for short periods of time is approximately 4 MV. Long-term storage at 53.1 MHz would require the tuning bias current supplies to operate at their maximum output current for very long periods of time. This kind of operation is beyond the safe operating limit of the supplies and is very wasteful of power and cooling capability. A better method must be

*The calculations were done with a numerical integration along the entire ring performed with a computer code PATRICIA[1] worked out at SLAC.

devised to tune the cavities to their maximum frequency. This could, for example, be a remotely operable mechanical device capable of being switched quickly between normal and storage operation. The Main-Ring cavities may require additional cooling for sustained high-power operation. It is comforting to realize that these problems are not unique to electron operation, but must be addressed for any beam storage.

Acceleration between 4 GeV and 12 GeV can be made slow enough to ease the requirements for the magnet power-supply ramp and the rf ramp. Although initially the acceleration could be made more rapid, toward the end it must slow down to make more voltage available to supply a reasonable rf bucket to the beam and to compensate for the energy loss. A net acceleration rate of 100 keV/turn will require about 1.6 sec.

The expected beam characteristics at the two energies of 4 GeV and 11.5 GeV are summarized in Table VIII-2. The beam sizes shown here are those in equilibrium with the synchrotron radiation, that is, after several radiation damping times.

D. Operation of the Main Ring at 4 GeV/c

Some years ago, it was possible to operate the Main Ring at a beam momentum of 8 GeV/c. Now it is normally run at approximately 9 GeV/c. Our scheme requires operation of the Main Ring at 4 GeV/c because this is the largest momentum one can expect for an electron beam accelerated in the Booster. There are obviously several concerns about operation at such low momentum.

It seems relatively easy to run the magnet power supplies at half the normal injection excitation. The magnets could be run with separate power supplies sources in a dc mode, if that were desirable, with very little power consumption. One could switch between the low-momentum mode and the normal injection mode relatively rapidly.

The main concern is in the quality of the Main-Ring magnets. The bending field equivalent ot 4 GeV/c is approximately 180 G. Assuming that the remanent field ΔB does not change, the relative variation $\Delta B/B$

Table VIII-2. Parameters for the Electron Operation of the Main Ring

Energy	4 GeV	11.5 GeV
Intensity	380 mA	380 mA
Revolution Period	20.96μs	20.96μs
Accelerating Frequency	53.105 MHz	53.105 MHz
No. of Bunches	1113	1113
Energy Loss	39 keV/turn	2.7 MeV/turn
RF Voltage	4 MV	4 MV
RF Shunt Impedance	9 MΩ	9 MΩ
RF Beam Power	15 kW	1.0 MW
RF Cavity Power	0.9 MW	0.9 MW
Power Amplifier		
Transmission Efficiency	0.5	0.5
Input Power Required	1.8 MW	3.8 MW
ε_H (95% of beam)	$0.024\ 10^{-6}\pi$ m	$0.20\ 10^{-6}\pi$ m
ε_V (95% of beam)	$0.051\ 10^{-6}\pi$ m	$0.42\ 10^{-6}\pi$ m
σ_E/E (rms)	2.1×10^{-4}	6.2×10^{-4}
Damping Times: Hor.	4.27 s	180 ms
Ver.	4.27 s	180 ms
Energy	2.13 s	90 ms
Synchron. Phase	0.215°	42°
Phase Oscill. Frequency	830 Hz	422 Hz
Bunch Length (rms)	2 cm	13 cm
RF Bucket Area	1.8 eV-sec	0.6 eV-sec
RF Bucket Height, ΔE/E	±1.8%	±0.46%

is now twice as bad as at 9 GeV/c, that is, the non-linear components (sextupole, octupole, ...) are twice as strong. On the other hand, because of the lower beam momentum, the correction system presently installed in the Main Ring is also twice as effective. Thus the two effects should to some extent balance off. It is obvious that a low-momentum mode of operation will require a new accelerator tune, which might require several shifts in the control room to develop, but little time in subsequent operation.

Assuming full coupling in the Booster, the beam emittance at 4 GeV is expected to be approximately 0.5π mm-mrad. The Main Ring is capable of accepting at least 1.5π mm-mrad at 8 GeV, with a tune of 19.4. It is quite possible that some increase of the beta function could somewhat shrink the Main-Ring aperture, but it should still be capable of capturing a 0.5π mm-mrad emittance.

Similarly, we observe that the betatron-oscillation damping time is 4.3 sec., which is quite large. The question is whether the beam can survive for the time required for filling the Main Ring, 15 sec. A crude measurement[2] of the proton-beam lifetime at 8 GeV has given about 20 sec. Measurements[3] of the lifetime at larger energies have shown a $1/p^2$ dependence on the beam momentum p. Recently is has been possible to measure[3] the increase of beam size with time but only at considerably larger energies; it would be difficult to try to extrapolate to find the behavior of a 4-GeV/c beam from these measurements. But, assuming that the beam growth is caused by scattering of the particles by the residual gas, the beam lifetime expected appears to be adequate for survival.

The final emittance of the electron beam is determined by the balancing effects of the diffusion processes that cause beam-size growth and of the radiation damping time τ, so one has

$$\varepsilon_\infty = \left(\frac{\sigma^2}{\beta}\right)_\infty = \frac{\tau}{2}\left(\frac{1}{\beta}\frac{d\sigma^2}{dt}\right),$$

where $d\sigma^2/dt$ is a measure of the diffusion effects. The contribution

from the synchrotron radiation to the vertical emittance is

$$(d\sigma^2/dt)_{rad} = 4 \times 10^{-7}\ m^2/s \text{ at } 4 \text{ GeV}$$

at a location where $\beta_V = 100$ m. At the same time, the beam lifetime is given by

$$\tau_\lambda = \frac{\tau}{2}\frac{e^\xi}{\xi} \quad \text{with } \xi = \frac{1}{2\pi}\frac{a}{\varepsilon_\infty},$$

where a is the ring acceptance. An acceptable lifetime at 4 GeV would be $\tau_x = 10^3$ sec. Assuming for the Main-Ring acceptance $a = 1.5\pi$ 10^{-6} m-rad, we derive the following limit on the beam emittance

$$\varepsilon_\infty \leq 8.3 \times 10^{-8} \text{ m-rad},$$

or in terms of the total diffusion coefficient

$$\left(\frac{d\sigma^2}{dt}\right)_{total} \lesssim 3.9 \times 10^{-6}\ m^2/\text{sec}$$

at locations where $\beta = 100$ m. Subtracting the contribution from the synchrotron radiation, one finally obtains a limit on the diffusion coefficients from other sources, such as scattering by the residual gas,

$$\left(\frac{d\sigma^2}{dt}\right)_{gas} \lesssim 3.5 \times 10^{-6}\ m^2/\text{sec at } 4 \text{ GeV}, \ \beta = 100 \text{ m}$$

which is at least one order of magnitude larger than what one would derive by scaling in momentum of observations made with a 200-GeV proton beam. Simple calculation of the gas-scattering diffusion coefficient gives[4]

$$\frac{d\sigma^2}{dt} \simeq 1 \times 10^{-6}\ m^2/\text{sec at } 4 \text{ GeV } (\beta = 100 \text{ m})$$

for a nitrogen pressure of 5×10^{-8} torr.

The time needed for filling the Main Ring is long enough that the first few batches are damped down to the equilibrium sizes, whereas the few last batches will not have the time to experience radiation damping. Thus, at the end of the filling, just prior to starting the

acceleration, the size of the beam will change from bunch to bunch. As one can see by comparing Tables VI-1, VI-2, and VIII-2, the emittances and the dimensions of the beam are larger at injection than at equilibrium. In particular, the energy spread, before as well as after, is small enough to be easily accommodated in the expected momentum aperture of the Main Ring ($\gtrsim$ 0.5%).

E. Main-Ring Vacuum

Storing electrons in the Main Ring will put an extra burden on the Main-Ring vacuum system because of desorption of gas molecules from the stainless-steel beam pipe by synchrotron radiation.

The Main-Ring vacuum system consists of unbaked stainless-steel pipe of approximately rectangular cross section, approximately 5 cm x 10 cm, with 30 ℓ/sec sputter-ion pumps spaced every 6.2 m (every bending magnet). In a lumped system consisting of pumps of speed S(ℓ/sec) separated by tubes of conductance C(ℓ/sec), the average pressure is

$$\bar{P} = \frac{Q_o}{S} \left(1 + \frac{S}{12C}\right) \text{ torr},$$

where Q_o (torr-ℓ/sec) is the gas load per pump, assumed to be uniformly distributed. For the Main-Ring vacuum pipe, C is approximately 6 ℓ/sec. In a typical operating mode, an average pressure of 5×10^{-8} Torr is measured,[5] which gives a calculated gas load of 10^{-6} torr-ℓ/sec per pump, that is, in a length 6 m. This load is a measure of the states of cleanness of the vacuum chamber and of the leaks.

The synchrotron radiation will augment the gas load Q_o. When electrons are stored in the Main Ring, the synchrotron radiation will desorb gas in a narrow band in the plane of bending. At first, this desorption might be very large, depending on the state of the surface of the vacuum chamber, and the pressure could climb to a point where the accelerator cannot be run. After some running time, however, the wall will become conditioned and the desorption rate will fall. Experiments at SLAC[6] have shown that the major contribution to gas desorption is by a

two-step process. The synchrotron-radiation x-rays knock out an electron from the wall. That electron, if it is energetic enough (above approximately 20 eV) will desorb a gas molecule when it returns to the wall.

The number of synchrotron radiation photons emitted per second may be estimated with a numerical integration over the spectrum. We find

$$N_\gamma/\text{sec} = 8.0 \times 10^{20}\ IE \quad \text{photons/sec},$$

where I is the average beam current in A and E the energy in GeV. The desorption coefficient, which gives the number of molecules desorbed per photon, is a function of the photon energy. The energy dependence is determined from observations in several electron rings, such as SPEAR, CEA and ACO. One can summarize the findings as follows:[7]

(i) for photon energies below 20 eV, the desorption is negligible;

(ii) the desorption coefficient increases up to a photon energy of the order of 1 keV. The average value in this range is about 2.5×10^{-5} molecules/sec.

(iii) For energies larger than 3 keV, the desorption decreases about linearly with the inverse of the photon energy. At 3 keV, one has about 4×10^{-5} molecules/sec.

(iv) For extremely large energies u, say about 10 times the critical photon energy u_c, the effect becomes negligible again. This behavior is an average over observations with different vacuum-chamber materials (stainless steel, aluminum, ceramic) and we shall adopt it for our estimates of the Main-Ring Vacuum.

In Table VIII-3 we show for comparison the radiation spectrum for two accelerators, PEP and Main Ring. The critical energy in the Main Ring is about 5 keV in the regular bending sections and 50 keV in the beam-crossing region, where the vertical bending magnets have a smaller bending radius. From Table VIII-3, one can see that most of the radiation is in the 0-3 keV region. It therefore seems safe to adopt an average desorption coefficient of 2×10^{-5} molecules/sec over the entire

radiation spectrum. This then gives a gas load due to radiation desorption of

$$Q_o = 2 \times 10^{-6} \text{ torr-}\ell\text{/sec per pump,}$$

which is twice the load due to leaks. There are plans at this time to improve the Main-Ring vacuum system by finding and eliminating as many leaks as possible. Then the synchrotron radiation desorption will be dominant. Eventually, an average vacuum of 10^{-7} torr with an 0.38-A, 12-GeV electron beam should be within reach. Observe that one may conclude from these considerations that a conditioning period, during which the pipe walls are bombarded by photons, may not be required. In addition, no major effects are expected at low energy. The vacuum degeneration will occur in the storage mode at 12 GeV. During 4-GeV injection one can assume the standard vacuum.

Table VIII-3. Synchrotron-Radiation Spectrum and Desorption Coefficients

Photon Energy (u)	PEP	Main Ring	D mol/sec
$\leq$ 20 eV	9.5%	20%	--
20 eV-3 keV	50	77	2.5×10^{-5}
3 keV - $10u_c$	40.5	3	~ 1/u
> $10u_c$	10^{-3}	10^{-3}	--

The previous considerations are based on very few measurements of gas desorption and on a very simple model. We believe that the actual effect of the synchrotron radiation on the Main-Ring vacuums can only be evaluated by direct observation, for example, by exposing a sample of the vacuum chamber to radiation.

Another of the effects of massive doses of synchrotron radiation is to destroy organic material. It is customary to have a shield in electron machines to absorb the synchrotron radiation before it can penetrate into the coil region of the magnets, or to design the magnets in

such a way as to exclude organic material, mainly epoxy and insulation, from the bending plane.

The Main-Ring magnets have epoxy in the median plane; it is shielded from the beam by a layer of stainless steel only 1 mm thick. Counteracting this unfortunate circumstance, we have two effects in our favor:

(i) the characteristic photon energy is low, so that the cross section is overwhelmingly photoelectric, and

(ii) the angle of incidence is very small, so that photons must be Compton-scattered to get out of the beam-pipe wall.

Assuming that the electrons that interact in the beam pipe wall by photoelectric effect are absorbed, the only power that gets into the epoxy is from photons that are Compton-scattered at large angles.

The total radiated power in the Main Ring is 1 MW or $2W/cm^2$. For an average β of 70 m and a typical photon emission angle of $1/\gamma$, the photons hit the beam pipe wall in a strip a few mm high, giving a power density $P_\gamma \approx 10W/cm^2$. The average angle of incidence on the pipe wall is 11 mrad, which means that photons that do not scatter have to penetrate a meter of steel. For ease of calculation,[8] we will assume that the power that leaves the wall in any energy interval is just the fraction of power in that interval times the ratio of Thomson to photoelectric cross section, multiplied by a solid-angle factor, which we take to be a quarter of the amount of the scattered radiation absorbed in 1 mm. This is clearly an overestimate of the radiation dose, since it does not take into account the absorption of energy by the photoelectric effect before the scattering.

Assuming that the photon total cross section in carbon is a factor 100 less than in iron and that for photons of 50 keV the absorption length in carbon is about 25 gm, we calculate that we will put at most 5 ergs/g-sec into the epoxy, or 0.05 rads/sec. For a limit of 10^8 rads before damage, this gives a lifetime of 2×10^9 seconds, or 50 years of

continuous running. Radiation damage from the synchrotron radiation is therefore not a problem.

F. Electron-Beam Lifetime

We have seen above that the electron beam survives for the time required to fill the Main Ring. The question is now whether the beam can survive the long period of time needed to perform ep scattering experiments at 12 GeV.

There are several factors that can contribute to the beam-size growth and beam lifetime. The dominant one is obviously the synchrotron radiation itself. About 1,500 photons are radiated in each turn per particle, with an average energy of about 2 keV. The spectrum drops very rapidly on either side of this energy. At 12 GeV, the quantum diffusion coefficient at locations where $\beta = 100$ m is

$$d\sigma^2/dt \simeq 10^{-4}\ m^2/sec,$$

two orders of magnitude larger than the contribution from gas scattering at 5×10^{-8} torr and much larger than any contribution from other effects, such as intra-beam scattering and bremsstrahlung on the residual gas. Thus the synchrotron radiation is the predominant factor in beam diffusion. Yet, when the spectra of the various effects are compared at energy transfers so large that one kick is enough to remove the particle from the aperture, the bremsstrahlung effect is much larger than all others and the beam lifetime seems to be primarily determined by it. Intra-beam scattering is very weak; as we have seen, the Touschek lifetime is of about 100 hours at 4 GeV and practically infinite at 12 GeV. In the classical approximation the lifetime τ_B due to bremsstrahlung is given by[9]

$$\frac{1}{\tau_B} = \frac{16}{3}\,\delta\,\frac{2^2mc^2}{\hbar}\,r_o{}^3\ln\left(\lambda\frac{192}{Z^{1/3}}\right)\ln\left(\frac{1}{\Delta}\right),$$

where δ is the residual-gas density

$$\delta = 3.2 \times 10^{16}\ P_{torr}\ cm^{-3} \text{ (room temperature)}$$

and Δ is the relative energy aperture. If we take $\lambda = 1$, $Z = 7$, and we apply the relitivistic correction we get a lifetime of 50 min for a pressure of 10^{-7} torr. This lifetime depends very crucially on the pressure, which in turn depends strongly on the amount of synchrotron radiation. This is by far the most strigent limitation we have found in our study of the electron-proton colliding-beam scheme.

Bremsstrahlung occurs also by scattering of electrons on the proton beam with which they are intended to be colliding. The lifetime τ_{BB} from beam-beam bremsstrahlung is given by

$$\frac{1}{\tau_{BB}} = \frac{16}{3} \frac{L}{N_e} \frac{e^2}{\hbar c} r_o^2 \ln \frac{1}{\Delta} \left(\ln(2\lambda\ \gamma_p \gamma_e) + \frac{1}{2} \ln \frac{1}{\Delta} \right).$$

where L is the luminosity and N_e the total number of electrons. For a luminosity of 10^{32} $cm^{-2}sec^{-1}$, the lifetime is about 16 days, comfortably long.

Two more limitations to the electron beam lifetime comes from the radiation quantun fluctuation itself. For a total energy loss of 2.7 MV and 4-MV rf voltage, the bucket height at 11.5 GeV is $\Delta E/E = \pm 0.46\%$. This would lead to a practically infinite lifetime for a relative rms energy of the beam of 6.2×10^{-4}. In Table VIII-4 we give the lifetime of the electron beam due to energy fluctuations versus the beam energy for 4-MV rf voltage.

Table VIII-4. Electron Beam Lifetime Due to Quantum Energy Fluctuations

E_{GeV}	U_{MeV}	τ_{damp}	σ_E/E	$\Delta E/E$	Lifetime
11.0	2.2	103 ms	0.060%	±0.60%	∞
11.5	2.7	90 ms	0.062%	±0.46%	40 years
12.0	3.2	79 ms	0.064%	±0.31%	7 min

This table shows the rapid variation of the beam lifetime with beam energy. Operation at 12 GeV is obviously not possible unless the rf voltage is raised to 4.5 MV by the addition of two more cavities. This justifies our original choice of 11.5 GeV for the electron beam shown in Table VIII-2. Actually, one should take the Main-Ring momentum aperture, rather than the momentum height $\Delta E/E$ of the buckets as shown in Table VIII-4 for the beam-lifetime calculations.

A lifetime of 50 hours requires a momentum aperture about 6 times the beam rms spread σ_E, that is, $\Delta E/E = \pm 0.36\%$. Such a value has been achieved in the Main Ring.[10] The correcting sextupoles with the addition of spacers between their coils were adequate for correction of the kinematic chromaticity of -23 and the remanent field non-linearities as well. With the low-beta insertion and the higher tune, the chromaticity is doubled, but we have confidence that the sextupole correcting system in the Main Ring is still capable of providing the momentum aperture required.

Another very strong limitation to the beam lifetime comes from the quantum-fluctuation effect on the betatron oscillations. In absence of coupling, the vertical beam emittance is twice as large as the horizontal one, and if one takes $1.5\pi \cdot 10^{-6}$ m-rad for the Main Ring acceptance, the beam lifetime would be only a few minutes. On the other hand, if there is full coupling between the two modes of oscillation, the vertical emittance would reduce by 50% and the horizontal increase by the

same amount, and the estimated lifetime becomes a few hours. Thus, full coupling in the Main Ring is crucial. The Main Ring has a total of 18 skew quads, each capable of an integrated gradient of 320 G. Their use, combined with the capability of changing tunes with trim quads, should enable us to reach full coupling. The lifetime is still very sensitive to the available betatron acceptance and successful operation will require very careful compensation of the closed orbit, continuous checking of the magnet alignment, and adequate control of the nonlinear remanent magnetic field.

G. Beam-Stability Considerations

An average current of 380 mA corresponds to 5×10^{10} electrons per bunch, about twice the number of protons the Main Ring can presently accelerate. Most of the considerations of Chapter VII apply also to stability of the electron beam. We have already developed tools in the Main Ring to cope with instabilities that involve coherent bunch motion, either transverse or longitudinal. The main concern is the individual-bunch lengthening and widening, similar to that observed with proton bunches. For an estimate of this effect, one can again make use of the stability condition (V-5) which we write in a slightly different form. We define the bunching factor B as the ratio of the peak current to the average current and observe that there is a simple relation between the rms bunch length σ and the relative rms momentum spread δ. Then we have

$$\left|\frac{Z}{n}\right| \lesssim 14 \frac{E}{e} \frac{\sigma\delta^2}{\ell I_{av}\gamma_T^2} , \qquad \text{(VIII-1)}$$

where $\ell = 5.65$ m is the separation length between bunches. With $\sigma = 13$ cm and $\delta = 0.62 \times 10^{-3}$, the impedance that can be allowed is 6 to 7Ω for 380 mA. This impedance is about five times less than what is observed in the Main Ring (see Section VII.B.). This fact would cause the beam momentum spread to increase until eq. (VIII-1) is satisfied for the actual impedance. Indeed, because of the synchrotron-radiation damping, it is believed[11] that individual electron bunches, which are

unstable at the beginning, will grow to a final spread δ_{th} that corresponds to the threshold (VIII-1), whereas proton bunches will grow to a final spread δ_{fin} given by the so-called overshoot formula

$$\delta_{fin} \cdot \delta_{in} = \delta_{th}^2,$$

δ_{in} being the initial spread. As a consequence, taking 35Ω and 380 mA, the electron beam spread should grow by 70%. In this case, the beam lifetime becomes approximately 1 min. Widening of the momentum acceptance would not help much because of the limited bucket height. This height can be increased only by doubling the number of rf cavities. Thus the only possible cure would seem to be scrupulous bookkeeping of Main Ring impedances and their reduction by a factor five. On the other hand, as discussed in Chapter VII, our observations on bunch lengthening in the Main Ring have been preliminary and require confirmation.

A final consideration concerns the energy loss to parasitic modes. The peak beam current is about 6A, two or three times larger than that now obtained with protons at large energy. We have indication, though not very definite, that the proton beam in the Main Ring suffers some energy loss[12] of rather obscure origin when the Main Ring is operated in the storage mode at high energies. If these losses are related to parasitic modes, one would expect a loss of a few hundred kilovolts for the electron beam of 380 mA at 12 GeV. In principle, this loss does not cause an increase of the momentum spread, but a reduction of the rf bucket size and hence of the beam lifetime. If no other effect is added, one can tolerate at most an extra loss of 400 kV, which would correspond to a lifetime of 4 hours. We expect a loss half this figure.

In summary, we have learned that the lifetime of the electron beam is the largest concern for us. It appears that operation of the Main Ring with electrons over a period of an hour is possible, but only with very delicate and sensitive tuning of the accelerator.

References (VIII)

1. H. Wiedemann, PEP-220, Sept., 1976.
2. F. Turkot, private communication, Fermilab, 1975.
3. I. Gaines, Proc. of the 1977 Aspen Summer Study on Colliding Beam Physics at Fermilab, Vol. 1, p. 115.
4. S. Snowdon, TM-341, Fermilab, Jan., 1972.
5. E. Fisk, S. Pruss, F. Turkot, private communications, Fermilab, 1977.
6. V. Cummings, et al., Vacuum Systems for Stanford Storage Ring, SPEAR, SLAC-PUB-797, Spet., 1970.
7. H. Winick, Proc. of the 1973 Aspen Summer Study on Colliding Beams, Vol. 2, p. 81.
8. P. J. Limon, Proc. of the 1977 Aspen Summer Study on Colliding Beam Physics at Fermilab, Vol. 2, p. 333.
9. J. D. Jackson, Classical Electrodynamics, John Wiley and Sons, Inc., New York-London, June, 1963, Chapter 15.
10. R. Stiening, et al., Proc. of the 1975 Particle Accelerator Conference, Washington, March, 1975, p. 1934.
11. A. G. Ruggiero, DESY PET-76/08, Hamburg, Sept., 1976.
12. A. V. Tollestrup, Proc. of the 1977 Aspen Summer Study on Colliding Beam Physics at Fermilab, Vol. 1, p. 97.

IX. e-p COLLIDING-BEAM PERFORMANCE

A. The Interaction Region

This region was discussed in Section VIII.A. Here we give more details relative to the interaction region.

The two upstream vertical bending magnets will produce a copious beam of photons directed toward the crossing point in the middle of the long straight section. The critical photon energy is 50 keV and the radiation loss is 175 keV per particle per magnet. Thus at every passage of an electron bunch, there will be a stream of 5×10^{11} energetic photons toward the central region. These photons must be stopped before they reach the area surrounded by the major detector in the colliding-beam region. Otherwise they will trigger the experimental apparatus and swamp the real events with a huge background.

Synchrotron-radiation shields are placed as sketched in Fig. VIII-1. The radiation coming from the magnet from the far end is effectively shielded by the innermost magnet, which has a vertical aperture large enough so that the photons will not hit the vacuum-chamber walls but instead will hit the outer side of the first shield between the quadrupole and the bending magnets. This shield will also capture a large fraction of the radiation from the second bending magnets. It extends to 4 cm from the horizontal bend plane and lets pass only the photons radiated during the last 2.5 m of bend. The vertical dipole is lowered by 5 cm to let the photons strike the shield rather than the pipe walls.

A second shield is placed between the two low-beta quads and extends to 3 cm from the horizontal bend plane. Finally, a third shield is located between the detector and the first quad, 5 m away from the collision center. This shield extends 2 cm from the beam axis. The three shields together can then stop 95% of the total radiation. It is true that 5% of the original number of photons is still a larger number (2.5×10^{10} per bunch), but they originate at shallow angles and making

the vacuum pipe 12 cm wide will comfortably allow them to pass the interaction region and strike the walls well beyond this point without causing triggers in the experimental apparatus.

These shields (or masks) are tantalum plates a few millimeters thick. Tantalum is favored, in spite of its high fluorescence yield, because of the relatively high energy of its k-absorption edge. There radiated photons are of 55.7 keV energy, about the critical energy of the radiation. It should also be observed that these energies are not easily absorbed in an ordinary detector. The masks will have their own mechanical-adjustment capability so that they can be inserted the right distance without limiting the beam lifetime.

The other problem relevant to the crossing region is the accuracy with which the two beams can be made to collide with each other. The difference in velocity is so small that it can be easily adjusted with small rf bumps. The two beams are made to collide at the desired location by continuously sliding the phase of one rf system relative to the other. For compensation of the closed-orbit distortions and adjustment of the horizontal crossing angle, few trim vertical and horizontal dipoles are located as shown in Fig. VIII-1. The insertion allows operation at beam energies varying over a wide range almost independently of each other. Changing the beam energies can cause vertical movement of the crossing point but by no more than half an inch.

B. Beam Separation

The two beams share about twenty meters of path in the interaction region. Unless they cross at an angle, this will cause three or four pairs of bunches to overlap at any time. The angle must be large enough so that bunches are separated at a point half an rf wavelength away (2.8 m) from the crossing center. One can consider the two bunches to be separated when, first, their mutual electromagnetic interaction is so small that its effect on the lattice and beam stability is negligible, and, second, when the overlapping of their tails does not cause

scattering events that significantly affect the detector counting. We state the following somewhat arbitrary numerical criterion: the two beams are separated when the sum of the rms bunch width is six times larger than the distance between their centers. This condition is independent of where the overlapping occurs because both beam size and beam separation increase linearly with distance from the crossing center. The ratio of the two quantities gives the crossing angle. The factor of six we have taken is certainly safe; it could probably be lowered to three, which corresponds to 0.3% of particle population overlapping and to a rather insignificant beam-beam effect. From these considerations, we choose a total crossing angle of 2 mrad. This angle cannot be reduced by eliminating one or a few bunches, unless the number of missing bunches is three or more, in which case the collision could also occur head-on.

C. Luminosity and Beam-Beam Tune Shift

In the approximation that the β function does not change across one bunch length, the luminosity is

$$L = \frac{N_1 N_2 \; f/2\pi}{\sqrt{a_1^2 + a_2^2} \; \sqrt{(b_1^2 + b_2^2) + (\sigma_1^2 + \sigma_2^2)\; \theta^2}} \; ,$$

where N_1 and N_2 are the number of particles per bunch in beam 1 and beam 2, repsectively, f is the frequency of bunch encounters at the crossing point, 2θ the total crossing angle, and a, b, σ are respectively the standard deviations of the bunch width, height and length at the crossing point. If each beam is made of N_B bunches, the frequency of encounter f is N_B times the revolution frequency f_o.

The beam parameters at the crossing point are shown in Table IX-1. We have assumed full coupling between horizontal and vertical betatron oscillations in the Main Ring. A crossing angle of 2 mrad is, in our case, a large angle. The luminosity is basically proportional to the inverse of the crossing angle times the proton bunch length, which is

also considerably larger than the electron bunch length. The luminosity shown in Table IX-1 has been calculated assuming 10-turn stacking in the Energy Doubler. With only one turn, the proton beam intensity is ten times lower, but the bunch length is also considerably less and the luminosity is only one third smaller, large enough for first-stage experiments.

The beam size does not change appreciably across the bunch length. Assuming a Gaussian distribution of particle in both beams, the luminosity per unit length also has a Gaussian distribution with an rms length of 9 cm. In the case of head-on collision, the rms length becomes about 26 cm (or 9 cm for single-turn injection in the Energy Doubler).

The beam-beam tune shifts of beam 1 due to beam 2 are given by

$$\Delta\nu_{x1} = \frac{r_1}{2\pi} \frac{N_2 \beta^*_{x1}}{\gamma_1 \bar{a}_2 (b_2 + \bar{a}_2)}$$

and

$$\Delta\nu_{y1} = \frac{r_1}{2\pi} \frac{N_2 \beta^*_{y1}}{\gamma_1 b_2 (\bar{a}_2 + b_2)} ,$$

where r is the classical radius of the particle and

$$\bar{a}^2 = b^2 + \sigma^2 \theta^2$$

The tune shifts are also shown in Table IX-1. Those for the proton beam are five times smaller than the canonical value of 0.005. The vertical tune shift for the electron beam is about a factor of three smaller than that now generally considered to be acceptable (0.06). Even for head-on collision (θ=0), the tune shifts do not get much larger; the worst case is for the proton beam in the horizontal plane, where a shift as 0.01 is expected. This is twice as large as the canonical value and one might expect some deterioration of the proton-beam lifetime, but it is not a major concern for us, because we are limited by the electron-beam lifetime, approximately an hour.

Crossing at an angle can be avoided by eliminating two bunches in a

Table IX-1. Beam Parameters at the Crossing Point

	Electrons	Protons
Energy	11.5 GeV	1000 GeV
β_x^*	35 cm	5.0 m
β_y^*	30 cm	5.0 m
η_x^*	1 cm	0.7 m
η_y^*	-6 cm	---
$\epsilon_x = \epsilon_y$ (95% of beam)	$0.33\pi\ 10^{-6}$m	0.013×10^{-6} m
σ_E/E	6.4×10^{-4}	1.2×10^{-4}
σ (rms length)	13 cm	50 cm
a (rms width)	0.14 mm	0.13 mm
b (rms height)	0.14 mm	0.10 mm
N (part/bunch)	5×10^{10}	2×10^{11}
θ (half crossing angle)	1 mrad	
$a_1^2 + a_2^2$	0.036 mm^2	
$b_1^2 + b_2^2$	0.030 mm^2	
$(\sigma_1^2 + \sigma_2^2)\theta^2$	0.27 mm^2	
f_o	47.7 kHZ	
N_B	1113	
L	0.8×10^{32} $cm^{-2}sec^{-1}$	
Interaction Length (rms)	8.9 cm	
$\bar{a}$	0.19 mm	0.51 mm
$\Delta\nu_x$	4.5×10^{-3}	9.1×10^{-4}
$\Delta\nu_y$	0.019	1.2×10^{-3}

row every third bunch in both beams. The luminosity would them remain unchanged for the same population per bunch. It is required that the two beams are separated 8.4 m away from the crossing center. This can be accomplished by moving the inner two vertical bending magnets a few meters to the inside. Another possibility, which does not require magnet moving, is to eliminate three out of four bunches; in this case the luminosity changes to 0.6×10^{32} $cm^{-2}s^{-1}$ with the same bunch population. The desired bunching can easily be obtained for the electron beam by operating the Electron Cooling Ring at a lower harmonic number (either 8 or 6 rather than 24) and at lower linac current (130 or 100 mA). The bunches so obtained would then be simply transferred to the Booster and to the Main Ring, which would both still be operating at 53.1 MHz. Care must be taken to match rf buckets during the two transfers. Only three turns of momentum stacking would be required in the Energy Doubler. The final stack can then be bunched at either harmonic number 371 or 278. We leave out the details of this alternative operation, which could ultimately turn out to be very useful and should be investigated.

D. Operation at Other Energies

1. Variation of Proton Energy. The proton energy can be lowered from 1000 GeV to 100 GeV. The betatron beam emittances scale with the inverse of the momentum, and, assuming the rf buckets are large enough, the bunch length and height increase and decrease respectively by 78% from 1000 GeV to 100 GeV. Away from the crossing center, the proton beam size is considerably smaller than the electron beam even at low energies and the beam-separation condition is therefore not affected, especially the crossing angle.

Thus the luminosity will scale roughly with the inverse of the proton bunch length. At 100 GeV, it is a factor of two smaller than at 1000 GeV, (see Fig. II-4). For head-on collision, the luminosity will vary with the inverse of the proton emittance (with the same value of β^*) and will therefore decrease linearly with the proton beam momentum.

In this case, the luminosity decreases by a factor five between 1000 GeV and 100 GeV.

In either case, lowering the energy of the proton beam will cause an increase of the proton-beam size, and thus a decrease of the beam-beam tune shift seen by the electron beam. On the other hand, the proton beam-beam tune shift would increase; for crossing at an angle, one has a tune shift of 0.01 at 100 GeV, whereas for head-on collision, we are already limited at 1000 GeV.

2. Variation of Electron Energy. The design of the e-p scheme has been optimized for an electron energy of 11.5 GeV, based on the present rf, magnet and vacuum capability of the Main Ring. For larger energies, since the synchrotron-radiation spectrum shifts toward shorter wavelengths, the constraints on the vacuum are less tight and there is still margin for radiation tolerances in the magnet system. But the rf is the principal limiting factor. This has two aspects, the total voltage and the power required. Even in the limit of zero current, more voltage is required to compensate the radiation loss and supply adequate buckets for reasonably long lifetime. The amount of voltage required increases roughly with the fourth power of the energy. Thus, for instance, 30 MV/turn are required for 20-GeV electrons. Even if the voltage is there, one needs more rf power to accelerate the same number of electrons. If more rf power is not available, the electron current that can be stored is proportional to E^{-4}. At the same time, the natural emittance increases as E^2 because of the enhancement of the quantum fluctuations and the luminosity would therefore be proportional overall to E^{-6}. At 20 GeV, the luminosity is down to 3×10^{30} $cm^{-2}s^{-1}$. At larger energy, the electron-beam size is larger and the beam-beam tune shift is smaller for both beams. Thus, the tune shift does not cause any problem. The increased beam size, nevertheless, might have some unexpected effect on the beam lifetime.

For energies lower than 11.5 GeV, the electron beam size decreases,

by a factor of three down to the injection value of 4 GeV, and there are no rf limitations. The beam-beam tune shift does increase, but for the proton beam it would stay below the canonical value of 0.005 for crossing at an angle, and the limitation is already encountered at the standard energies for head-on collision. The electron beam tune shift would reach the stochastic limit at 4 GeV (~0.06) in either case. For the same electron-beam intensity (which could not be increased without making the self-field tune shift too large (see Section V.B.)), the luminosity could increase at most by a factor of two (see Fig. II-3), since it is basically determined by the proton beam size.

Operation of the Main Ring with the electron beam at very low energies is problematic. In fact, though the quantum lifetimes become longer, the gas-scattering effects of the vacuum predominate.

X. FUTURE DEVELOPMENT, SCHEDULE AND COST

A. Future Development

Several steps could be undertaken at a later time to increase the luminosity and center-of-mass energy, after exploitation of the initial performance of the scheme we have outlined in this report. In the long run, a new conventional ring for the electron beam could be designed and built aiming at energies of 20 GeV or more. This will depend a great deal on encouragement one might get from the discoveries of the first phase.

For instance, great benefit could come by using a beam of polarized electrons. The polarization time is given by[1]

$$1/T = \frac{5\sqrt{3}}{8} \alpha \frac{\hbar^2}{m^2c^4} \gamma^5 \frac{|\dot{v}|^3}{c^3} .$$

Since

$$\alpha = 1/137$$
$$v \sim c$$
$$|\dot{v}| = v^2/\rho$$

then

$$\frac{1}{T} = 3.5 \times 10^{-19} \gamma^5 \langle G^3 \rangle \text{ sec}^{-1}$$

where $\langle G^3 \rangle$ is given in Section VIII.C and is expressed in m^{-3}. At 11.5 GeV, the polarization time is approximately 1000 minutes, which is definitely too long, but it is 1 hour at 20 GeV and 20 minutes at 25 GeV. Thus, with a new ring especially designed for the electron beam, it would be possible to reach higher energies and eventually to use polarized beams.

Another useful application would be the injection of positrons rather than electrons. We have not investigated this possibility. It is not obvious where a target for the conversion should be located and what the production rate could be. A reasonable amount of positrons

could be collected only over a long period of time and would give reduced luminosity. Higher positron collection rate could only be achieved with a faster synchrotron injector. The Electron Cooling Ring itself could be ramped at least as fast as the Booster if the vacuum chamber could be removed.

What we have proposed in this report is only the first modest and economical experiment. The hope is that this will open a generation of e-p experiments at Fermilab which would become more and more sophisticated by adding more expensive equipment.

B. Schedule

It is difficult to make a schedule for an e-p colliding system because the scheme we have outlined depends on the acquisition of components that are presently under design or construction for other colliding-beam projects. The major item is of course the Energy Doubler, which is expected to be completed and operating by the beginning of 1981. The Electron Cooling Ring should be completed and operating by the end of this year (1978). There are thus two or three years to get ready for the first e-p experiment. Until then, one can start to make progress on two projects that are essential to the entire experiment:

(i) Operation of the Main Ring at 4 GeV/c; one can use protons at this stage, measuring their lifetime and the beam-size growth to extrapolate to the electron-beam size and lifetime. During this period, one would like to also conduct experiments on the Booster and Main Ring rf systems, to determine their capability of running cw at 53.1 MHz for very long periods of time.

(ii) In a second period, we suggest acquiring an electron linac to test the performance of the three rings (Electron Cooling Ring, Booster and Main Ring) with an electron beam. One could then learn the necessary rf gymnastic and beam transfer, as well as investigating the effect of the synchrotron radiation on the Main-Ring vacuum. For this second stage, the transfer line that joins the Booster to the Main Ring for reverse injection is needed.

C. Cost Estimate

Most of the cost of the project is for the acquisition of an electron linac and for the design and construction of the experimental detector. The rest is relatively toll free like the Energy Doubler itself which stands alone as a separate project, or the Electron Cooling Ring which is being built for different purposes. A few technical components nevertheless have to be added to make possible the operation of the system with electrons. Table X-1 gives a summary of the cost. The cost of the electron linac has been estimated by the ARCO Company, which is willing to make one for us, and install and test it in place. The breakdowns for the cost of the technical components and the two kinds of detectors are shown in Tables X-2, 3 and 4. Two generations of experiments are possible with detectors of different nature. For completeness, we have therefore included the cost of both. The cost of the detectors corresponds to those described in Chapter IV.

Table X-1. Summary of Cost Estimate

	Item Cost	Total Cost
Electron Linac	$1,400,000	
Technical Components	800,000	
Magnetic Detector	2,200,000	
Calorimeter Detector	2,200,000	
EDIA	1,000,000	
		$7,600,000
Contingency	$ 700,000	
Escalation	700,000	
		$1,400,000
		$9,000,000

Table X-2. Technical Components

		Total Cost
Linac Housing, Shielding and Power Supply		$ 150,000
Transport Line from Linac to ECR		20,000
Injection Kicker to ECR		10,000
RF Cavities for ECR		50,000
Power Supply to Ramp ECR		200,000
Radiation Shielding for ECR		100,000
Injection Kicker to MR		20,000
MR RF Cooling and other RF Modifications		50,000
MR Low-Beta and Crossing Injection:		
Six Quadrupoles	$75,000	
Six Vertical Dipoles	45,000	
Six Power Supplies	60,000	
Vacuum Chamber, Pumps	20,000	
		200,000
		$ 800,000

Table X-3. Magnetic Detector

24 Drift Chamber Planes	$ 410,000
2 pairs of x- and y- hodoscopes	90,000
Lead-glasses:	
(34 x 34: 3.5 in. x 3.5 in. x 14 in.)	1,200,000
Magnet	500,000
Total	$2,200,000

Table X-4. Non-Magnetic Detector

Drift Chambers:		
Electronics	$270,000	
Mechanical (24 planes)	135,000	
		$ 410,000
Lead-glasses:		
(3.5 in. x 3.5 in. x 14 in., including photo-tubes, bases)		1,200,000
2 pairs of x- and y- hodoscopes		90,000
Segmented Calorimeter:		
(40 layers of 1-in. steel and acrylic plastics, 1600 photo-tubes and bases, 8 collision lengths)		500,000
Total		$2,200,000

References (X)

1. V. N. Baier, Proc. of the Internat. School of Physics "E. Fermi", Course 46, 1971, p. 1.